# Consortium for Materials Development in Space

The University of Alabama in Huntsville
Huntsville, Alabama 35899

**Annual Report**
**Technical Section**
**Oct. 1, 1988-Sept. 30, 1989**
**NAGW-812**

**Industrial members of CMDS are:**

**Boeing Aerospace Company**
**Deere & Company**
**Frontier Research**
**IBM (Almaden Research Center)**
**Instrumentation Technology Associates**
**McDonnell Douglas Astronautics Co., Huntsville**
**Teledyne Brown Engineering**
**Thiokol Corporation**
**Wyle Laboratories**


Charles A. Lundquist,
Director

Francis C. Wessling,
Associate Director

Valerie Seaquist,
Assistant Director



**Submitted by the University of Alabama in Huntsville,**
**the legal entity responsible for establishing and operating the Consortium, to:**

**Office of Commercial Programs**
**National Aeronautics and Space Administration**
**Code CC**
**Washington, DC 20546**

## CONTENTS











**ON THE COVERS**

**Front:** A Starfire 1 vehicle boosts the Consort 1 mission out of the launch rails at the White Sands Missile Range in New Mexico. (U.S. Army photo)

**Back:** Francis Wessling and Samuel McManus show off the foam ball their experiment produced during the Consort 1 flight. (UAH photo)

# 1
# FISCAL YEAR OVERVIEW

ORIGINAL PAGE
BLACK AND WHITE PHOTOGRAPH

**Figure 1-1**
ITA's membership in CMDS added the Materials Dispersion Apparatus to the Consortium capabilities.

In initial plans made in 1985, the Consortium for Materials Development in Space (CMDS) embraced three specific concepts:

- Commercial materials development that benefit from unique attributes of space,
- Commercial applications of physical chemistry and materials transport, and
- Prompt and frequent experiments and operations in orbit.

These continue to be guiding concepts for the CMDS.

Commercial materials development is accomplished through several individual projects typically staffed by joint university-industry teams. Materials projects pursued by the CMDS, and the project team members, are listed in Table 1-1. These projects indeed involve applications of physical chemistry and material transport in the unique environment of space flight.

This fiscal year provided the first opportunity for flight experiments and operations. As Table 1-1 shows, the Consort 1 suborbital rocket mission carried five investigations to promote four of the projects. Later parts of this report summarize by project the results from this very successful flight. Table 1-1 also tabulates the demanding program of flight investigations planned for fiscal 1990 and beyond. Many preparations for these coming missions were necessary in fiscal 1989; subsequent parts of this report describe these efforts.

Initiation of two series of suborbital rocket missions became a commercial development in its own right. Its objectives are establishment and demonstration of commercial capabilities to prepare, integrate, launch, and recover suborbital payloads for materials and biotechnology experiments. In attaining these goals, the Consortium followed the schedule in Table 1-2. The capabilities and team organizations for the Consort and Joust missions are in Table 1-3. These suborbital options will be used extensively by the several Centers for the Commercial Development of Space (CCDS). The Consort and Joust capabilities are also available to paying customers outside the CCDS family, and the industry-UAH teams are publicizing this opportunity.

The suborbital rocket activity is one example of commercial infrastructure supporting the basic materials objectives of the Consortium. Another example is a Universal Small Experiment Container (USEC) being designed for facile use in Spacelab or Spacehab when either is carried aboard the Shuttle, as well as in the Shuttle middeck (Figure 2.2-2; page 9). The USEC has been designed by Wyle Laboratories in Huntsville as part of their contribution to CMDS objectives. Wyle will also market copies of the USEC to other organizations needing such containment for their flight equipment. The preliminary design review for the USEC was held Sept. 27, 1989. The CMDS plans to employ three of four USECs aboard the first flights of the U.S. Microgravity Laboratory (USML-1) and Spacehab in 1992.

Also planned for Spacehab 1, the Consortium is procuring from Boeing Commercial Space Development Co. a copy of the crystal growth furnace system that they have developed in connection with a Joint Endeavor Agreement with NASA. The furnace will be reconfigured slightly to accommodate it aboard Spacehab and to adapt it to the objectives of the CMDS investigations. The system will have three furnace modules, each containing two ampoules. For Spacehab 1, one furnace each will be dedicated to experiments for the Center for Commercial Crystal Growth at Clarkson University, the Center for Space Processing at Vanderbilt University, and the CMDS. Thus, in procuring the furnace system, UAH is acting on behalf of a group of CCDS's. The CMDS furnace modules will grow zinc se-

The University
Of Alabama
In Huntsville

# CMDS Materials Projects and Flight Opportunities

| Project | Industry Partner | Potential Products | Consort 1 (3/89) | Consort 2 (11/89) | LDEF-1 (1/90 recovery) | CONCAP-2 ('90) | GAS-105 (mid-'90) | Joust 1 (10/90) | EOIM-3 ('91) | USML-1 (10/92) | Spacehab 1 ('92) |
|---|---|---|---|---|---|---|---|---|---|---|---|
| Surface coatings and catalyst production by electrodeposition | McDonnell Douglas Space Systems Co. | Improved surface coatings and metal catalysts | ● | ● | | | ● | ● | | ● | ● |
| Physical vapor transport crystal growth | Boeing Aerospace | ZnSe electro-optical devices | | | | | | | | | ● |
| Non-linear optical organic materials | IBM & Teledyne Brown Engineering | Optical computers, electrooptical devices | | | | | ● | | | ● | ● |
| Demixing of immiscible polymers | Phillips Petroleum (guest investigator) | Blended polymers and separation of organic materials | ● | ● | | | ● | | | | ● |
| Nuclear track detectors | Frontier Research | Improved detector materials | | | | | ● | | | | |
| Materials preparation and longevity in hyperthermal oxygen | (Negotiations under way with prospective partner) | Spacecraft surface coatings | | | ● | ● | | | ● | | |
| Powdered metal sintering | Teledyne Wah Chang (guest investigator) | Composites of metals and refractory materials | ● | | | | | ● | | | |
| High-temperature superconductors | Lockheed, GE, LANL (Guest investigators) | Improved systems for commercial satellites | | | | ● | | | | | |
| Polymer foam formation | Thiokol Corp. | Lightweight space structures | ● | ● | | | | ● | | ● | |
| Iron-carbon solidification | Deere and Co. | Improved cast iron processes | | | | | | | | | |

**Table 1-1**

lenide (ZnSe) by the physical vapor transport technique.

As a service to potential new industrial users of NASA's ground-based facilities, Instrumentation Technology Associates (ITA), through the CMDS, has prepared two documents, Commercial User Handbook and Planning Guide for NASA Ground-Based Microgravity Facilities, and Typical Microgravity Experiment Data Results from NASA's Ground-Based Facilities. These will be reviewed and printed in fiscal 1990.

ITA also provided a Materials Dispersion Apparatus that flew on Consort 1 (Fig. 1-1). This unit, with provisions to support multiple experiments, was used on Consort 1 by several investigators through arrangements with ITA.

A new task initiated by the Consortium in 1989 is the commercialization of space fluid management. This is geared towards the control and transfer of fluids for use in space, and in the space environment. Initial

**Consort/Joust Procurement Schedule**

| | |
|---|---|
| Solicitation to industry | Feb. 15, 1989 |
| Preproposal briefing | Feb. 24, 1989 |
| Proposals received | April 10, 1989 |
| Evaluation | April 11-28, 1989 |
| Contracts awarded | May 5, 1989 |
| Consort 2 launch | Nov. 15, 1989 |
| Joust 1 launch | (Oct. 1990) |

**Table 1-2**

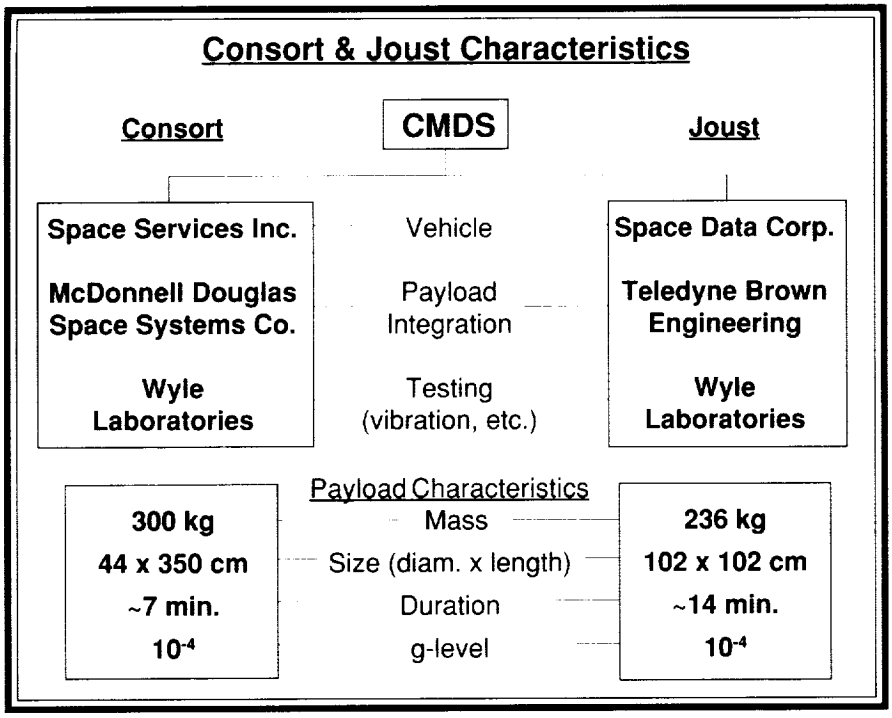


**Table 1-3**

**Table 1-4**

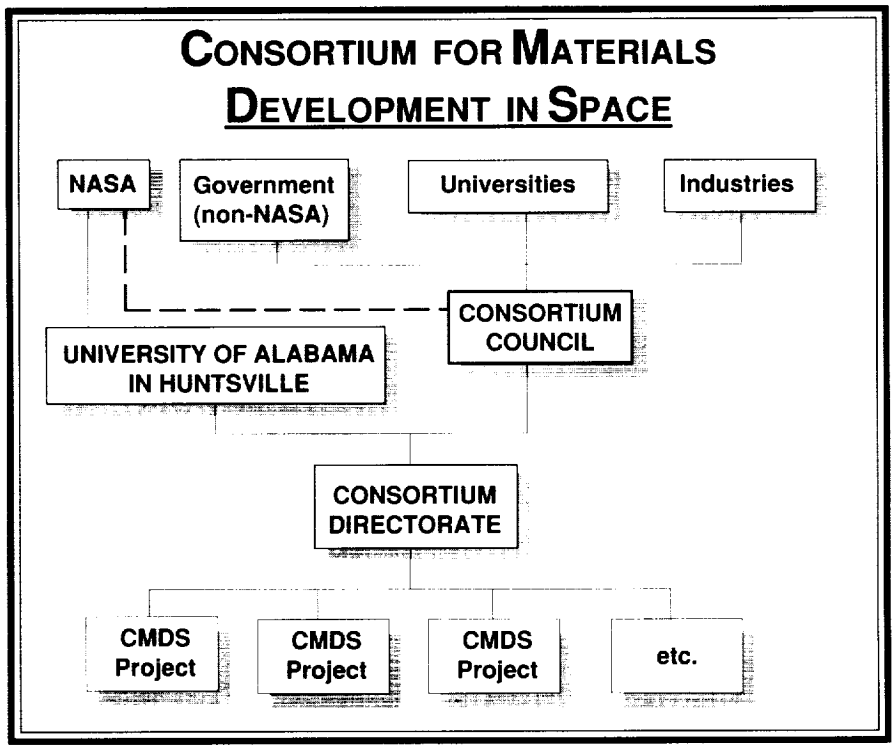


efforts will lead to a national conference on the subject in March 1990.

Administration of the Consortium in fiscal 1989 continued within the structure established in earlier years (Table 1-4). Toward the end of the year, arrangements were made to add a Consortium Assistant Director to accommodate the growing administrative workload associated with the increasing flight rate.

The Consortium Council met twice—on Dec. 14, 1988, and April 26, 1989. At the first of these, the Council acted on applications for new members. The Council accepted the application of Thiokol Corp. for membership with Council representation. They also approved the application of ITA for associate membership. Martin Marietta communicated its decision to discontinue work on atomic oxygen interactions with materials in space, and accordingly withdrew from Consortium membership.

The Council had its second business meeting at Guntersville (Ala.) State Park just preceding the annual review. As has become the custom, each project reported its progress as part of the Guntersville conference. These reports included early results from the Consort 1 flight.

As this overview demonstrates, fiscal 1989 has indeed been an active and productive year for the Consortium. Specific details can be found in the remainder of this report.

Key to the Consortium's development of materials "in space" are flight opportunities which place experiment payloads in space for periods ranging from minutes to days, then return them to Earth for analysis and development of follow-on experiments.

# 2 FLIGHT PROJECTS

## 2.1 SUBORBITAL CARRIERS

In 1988 CMDS and NASA's Office of Commercial Programs initiated planning for acquisition of commercial suborbital launch services to provide a range of early flight opportunities.

The key element in this activity was that the CMDS sought commercial launch *services*. The CMDS specified the payload mass and the period and level of "microgravity" desired. The contractor selected the vehicle and provided launch licensing and range services. This was analogous to purchasing an airplane ticket and having the airline provide the aircraft, flight services, etc.

Two suborbital launch programs are now active under the CMDS—Consort, initiated in 1988 and which had its first launch in March 1989, and Joust, which will have its first launch in the fall of 1990.

Teamwork is an important factor in the success of the CMDS suborbital program. In addition to the members of the Consortium and the launch services contractors, CMDS has been supported by three Huntsville firms: McDonnell Douglas Space Systems Co., Teledyne Brown Engineering (Consort and Joust payload integration, respectively), and Wyle Laboratories (verification testing).

### Consort program

The Consort program is designed to provide more than 7 minutes of "microgravity" at less than $10^{-4}$g for a 300-kg. (650 lbs.) payload. The payload itself is 43.8 cm (17.3 inches) in diameter and 350 cm (11.5 feet) tall. The Consort missions are launched by the Starfire I vehicle developed by Space Services Inc. of America in Houston, Texas (Fig. 2.1-1). Starfire I is a variation on the Terrier-Black Brant sounding rocket and other proven hardware designs. The primary difference is substitution of a more powerful Thiokol TX664-4 motor for the Terrier first stage.

Launch of Consort 1 took place on March 29, 1989, at the White Sands Missile Range in New Mexico. First and second stage solid rocket motors boosted the payload to an altitude of 301 km (187 miles). During the coast period above the atmosphere the payload experienced g-levels less than $10^{-4}$ g for 7 minutes. At the end of the coast period the payload was "spun up" to reduce re-entry heating effects. After re-entry, drogue and main parachutes were deployed, and the payload landed approximately 93 km (58 miles) north of the launch site about 14 minutes after lift-off. A special report on the Consort 1 flight is provided on pages 11-16.

Consort 2 is to be launched from White Sands in November 1989, with 12 experiments provided by CMDS plus three other Centers for Commercial Development of Space (CCDS): the Center for Advanced Materials at Battelle, the Center for Cell Research at Pennsylvania State University, and Bioserve Space Technologies at the University of Colorado. The payload includes five experiments and two accelerometer systems which flew on Consort 1 and seven new experiments, designed and developed since Consort 1. The intent is to phase in experiments from flight to flight so that each experimenter has an opportunity for two flights and to improve hardware and repeat earlier results.

The reflight experiments contained in the lower two-thirds of the Consort 2 payload are:

- Materials Dispersion Apparatus will allow several researchers the opportunity to study a variety of phenomena including bone marrow growth, organic cell growth

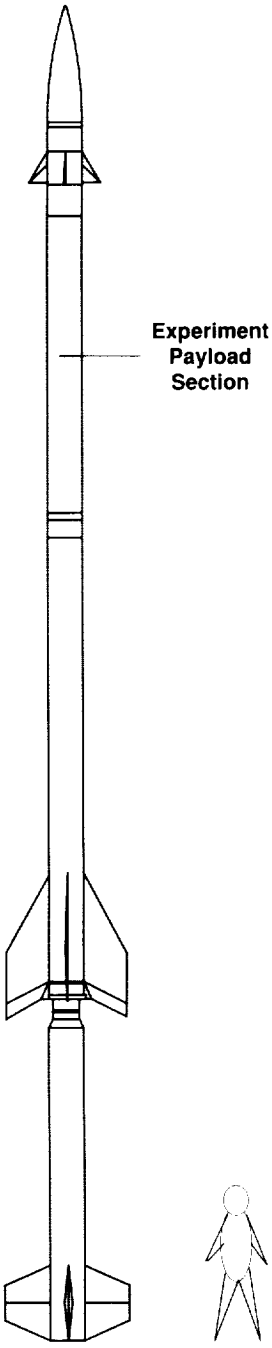


**Figure 2.1-1**
Consort launch vehicle

and diffusion phenomena. The small test chambers allow many researchers to perform experiments in a small volume.

- Demixing of immiscible polymers experiment will photograph the initial stages of demixing, and may be able to see some systems completely separated after their mixing in low-g. In addition, the effect of container shape and liquid contact angle on demixing can be photographed. Ultimately, this information will be used for biological cell separation (described on page 28).
- Electrodeposition apparatus will obtain samples of nickel and cobalt deposited over a range of current densities and also to obtain codeposited particles and metals for later analysis. These results may yield new forms of catalysts (page 17).
- Elastomer modified epoxy resins will yield samples processed in low-g that are adequate for determining the morphology of these resins, as well as provide specimens for tensile testing. New forms of epoxy may ultimately emerge (page 31).
- Foam formation apparatus will produce a sample of polyurethane foam with aluminum particles in low-g. This sample will be analyzed for cell morphology, thermal conductivity and compressive strength. The foaming process will be photographed during microgravity to assist in understanding the formation process. A better understanding of the foam formation process should result (page 45).
- Low-g, 3-axis accelerometer package and the UAH accelerometer package will measure g-levels during the flight (page 47).

Seven new experiments contained in the upper segment of the Consort 2 payload are:

- Improved Materials Dispersion Apparatus, based on the MDA described above, will carry additional biological experiments.
- Automated generic bioprocessing apparatus will provide an opportunity for studying biological reaction kinematics. This includes tubulin self-assembly into microtubules, fibrin polymerization and collagen polymerization, microorganism nutrient uptake, liposome formation and binding of rhizobia to plant root hairs (Bioserve Space Technologies).
- Biomodule will test cellular secretion which is the basis of cellular communication (Center for Cell Research).
- Polymer thin film apparatus will use ultraviolet light to cure a polymer liquid containing suspended aluminum flakes. The resultant thin film will be evaluated for the distribution of aluminum flakes and for optical and electrical properties (Thiokol Corp.).
- Polymer membrane processing will seek an understanding of the effect of convection-driven currents in the transport processes which occur during the evaporation casting of polymer membranes (Battelle Advanced Materials CCDS).
- Multiphase polymer curing will study phase dispersion in order to acquire a better understanding of the fundamental properties of thermoplastic and thermosetting composites (Battelle Advanced Materials CCDS).
- Plasma polymerization in microgravity will generate carbon particles or films from acetylene in a 10 kilohertz alternating current plasma. A photographic record will be made of the process (Battelle Advanced Materials CCDS).

Experiments are integrated into a payload module approximately 350 cm in length, 44 cm in diameter and weighing approximately 280 kg.

The entire payload module is sealed to maintain a pressure of one atmosphere throughout the flight. Three pressure-tight bulkheads are provided: one at the top of the payload, one at the bottom and one below the upper payload compartment. This provides two separate

compartments so that if one should leak the other would still maintain one atmosphere of pressure. The experiments are mounted on longerons which are attached to a bulkhead on one end and pinned on the other. This facilitates the integration of the experiments on the payload module, and permits an experiment to be assembled and tested on its own mounting plate.

The payload module provides power to the experiments through a Power Distribution and Control Unit (PDCU). During flight, the PDCU receives power from either of two battery packages and distributes it to payload experiments and support systems. During ground operations, the PDCU can also receive and distribute power from a ground power source via an umbilical. The PDCU provides for discrete experiment on/off control, current limiting and power usage monitoring as well as battery monitoring and charging.

The payload module sends lift-off and low-g signals to the experiments via a signal distribution board. The experiment serial outputs are transmitted through the ground umbilical and through telemetry. Experiments receive communications through the ground umbilical only. Experiment data are transmitted by the rocket to a ground station during flight and recorded on nine-track magnetic tape. Selected transmissions are sent to experiment monitors at the launch complex.

The mission profile for Consort 2 is expected to be identical to Consort 1.

### Joust program

After a contract competition in February 1989, Space Data Corp. of Chandler, Arizona, was selected to provide its Prospector vehicle for the Joust series. Prospector is based on the Castor IV-A booster developed for the Delta II launcher, and on other proven vehicle elements (Fig. 2.1-2).

The Joust series of launches will provide 14 minutes of low-g for a payload weighing 236 kg. (520 lbs.). The payload envelope is 102 cm (40 inches) in diameter and 102 cm (40 inches) tall.

Launches will be from the Eastern Test Range at Cape Canaveral, Fla., and will involve water recovery to the east of the Cape. Total flight time will be 27 minutes, including 14 minutes of experiment time at less than $10^{-4}$g. The payload will reach an altitude of more than 804 km (540 miles) and will splash down 54 km (34 miles) away.

The Joust 1 payload has three longitudinal longeron pairs on which the payload elements will be mounted (Fig. 2.1-3). This will allow payloads to be interchangeable with Consort.

The Joust 1 payload, slated for launch in the fall of 1990, is in definition at this writing.

### Payload support

The CMDS has designed both the Consort and Joust payload sections to provide several services to the experimenters, including:

- Power Distribution and Control Unit (PDCU) delivering 28-volt electrical power from NiCd F-cell batteries, discrete on/off control, current limits, and power monitoring,
- Experiment Interface Unit (EIU) allowing two-way communications with the payload over standard serial interfaces at 9,600 baud while on the ground. Lift-off and microgravity-onset signals also are provided to the payload, and data may be transmitted in flight,
- Three-axis accelerometer package with a resolution exceeding $10^{-4}$g,
- Access to the payload up to a few hours before launch, depending on experiment needs,
- Prelaunch payload temperature control by means of a styrofoam enclosure and air conditioning, and
- Recovery of the intact payload.

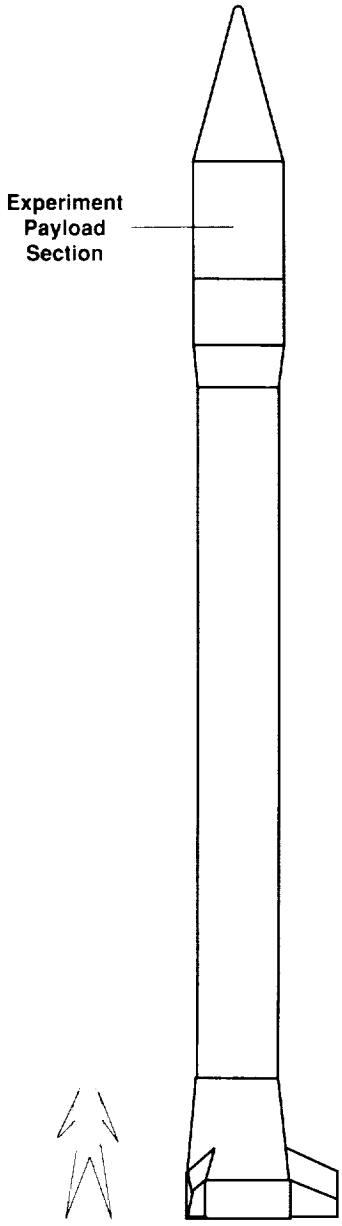


**Figure 2.1-2**
Joust launch vehicle

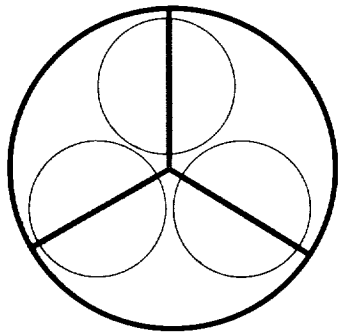

**Figure 2.1-3**
Joust cross-section shows how Consort-size payload elements (shaded) can be accommodated.

## 2.2
## ORBITAL CARRIERS

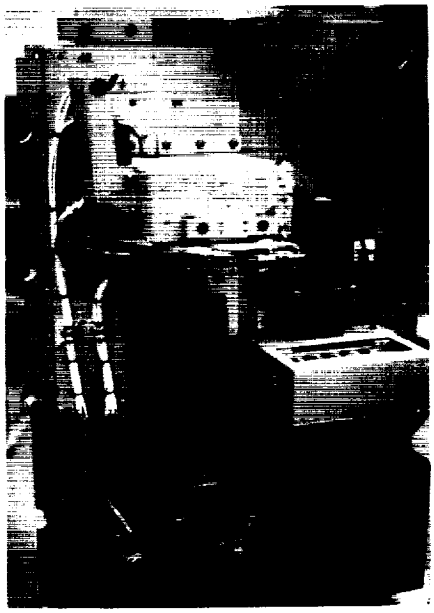

**Figure 2.2-1**
Interior of GAS-105 showing apparatus for electrodeposition on left side and demixing of immiscible polymers (without camera) at right.

ORIGINAL PAGE
BLACK AND WHITE PHOTOGRAPH

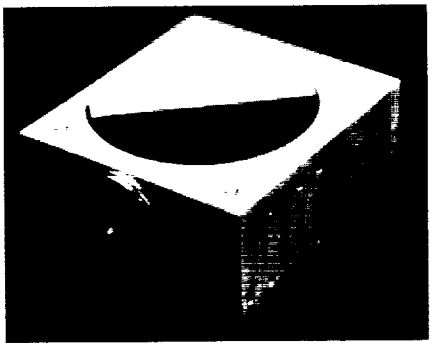

**Figure 2.2-2**
Reflectometer planned for use on CONCAP-2

Extended low-g time will be provided to CMDS experimenters in the 1990's by facilities carried aboard the U.S. Space Shuttle. Experiment hardware carried aboard the missions often have much design heritage in common with Consort and Joust hardware; other items will be unique to Shuttle. The principal differences are the period of low-g time, and the resources (power, data, volume, mass), available to the experimenter. Space Shuttle missions last a minimum of 4 days and, in the case of Spacelab payloads, may last up to 10 days or more. The entire flight period is not available to the experimenter, though. Such missions typically have large numbers of experiments requiring equal attention, and an individual experiment may be run for only a day or two. This still is more than two orders of magnitude greater than what is possible with suborbital carriers, and, when combined with additional resources, make shuttleborne facilities highly desirable.

Several CMDS experiments now under development will take advantage of the orbital carriers outlined presently.

### Getaway Special

The Small, Self-Contained Payload—popularly known as the Getaway Special—an independent payload mounted in the Shuttle payload bay. A Getaway Special uses a canister-shaped container 48.3 cm (19 in.) in diameter and 50.8 cm (20 in.) tall; payload mass may be up to 91 kg (200 lbs.). Normally it is fully autonomous and takes only on/off commands from the flight crew. This "small" capability has been used by many experimenters in "proof of principle" demonstrations before scaling up to larger experiments.

As now configured, Getaway Special 105 (GAS 105) contains equipment to support four CMDS projects. Initial planning for GAS 105, predating establishment of the Consortium, and embraced a joint effort between UAH and the Space & Rocket Center as a sequel to GAS 007 flown successfully on the STS 61-C mission in 1985 (Fig 2.2-1). GAS 007 carried out several student experiments and a communications experiment for the Marshall Space Flight Center Amateur Radio Club. As part of this heritage, a single student experiment is included in GAS 105. Also, several electrical and mechanical support systems are derived from systems provided on GAS 007.

Four of the Consortium experiments on GAS 105 utilize the microgravity environment of space, and one requires exposure to the radiation environment. Consortium investigations are:

- Separation of immiscible polymers (page 28),
- Nonlinear optical organic thin films (page 24) and crystals (page 23),
- Electrodeposition and codeposition (page 17), and
- Nuclear track detector materials, (page 32).

The scientific investigations involved in each of these is described on the indicated pages; details of the flight projects are in the CMDS 1988 report.

During this year the final safety data package was submitted to NASA for review and approval. Components of GAS 105 are now in final assembly and test.

Flight readiness of GAS 105 is scheduled for the spring of 1990. This anticipates that a flight opportunity is likely in the summer of 1990.

An exciting extension of the GAS concept is the Complex Autonomous Payload (CAP) program which allows GAS-type payloads to be flown with higher priority. CONCAP-2—the Consortium Complex Autonomous Payload—will carry two types of experiments concerning materials surface reactions resulting from exposure to the low Earth orbit environment.

Materials facing into the velocity vector (i.e., the "windward" side) of

a spacecraft are exposed to a flux of atomic oxygen at energies around 5 electron volts (eV). In addition to significant implications in the selection of protective surfaces for spacecraft, this flux can also be used in the treatment of specialized materials. CONCAP-2 will use a GAS can with a lid that opens in orbit to expose several classes of samples plus four flux measurement devices.

The first CONCAP experiment will expose samples of high-temperature superconductors (HTSC) to the atomic oxygen flux. Experiments at the Los Alamos National Laboratory have shown that oxygen-deficient HTSC films ($YBa_2Ca_3O_{7-x}$) could be converted to high-performance materials by processing in hyperthermal oxygen. The study of the physics and chemistry of such surface interactions is the subject of an on-going investigation at the CMDS.

For CONCAP-2, superconductor materials will be prepared and characterized on the ground, exposed to the atomic oxygen environment in space, then recharacterized on the ground after flight. A subset of the samples will be mounted on a hot plate to hold their temperature at 300 to 320°C. Reflectometers (Fig. 2.2-2) will measure how oxygen from the space environment is scattered off exposed surfaces. The design was proven on the STS-8 Shuttle flight in 1983.

The second CONCAP experiment involves preparation and longevity of other materials in hyperthermal oxygen. Several samples of passive materials will be carried to predict materials degradation on spacecraft, acquire accurate data on materials reaction rates in the space environment, test oxidation-resistant coatings for commercial use, develop new materials based on energetic molecular beam processing, and advance the fundamental understanding of fast atom interactions at surfaces.

The experiments require 4 to 10 hours of exposure to the space environment with the Space Shuttle payload bay pointed into the velocity vector. Flight tentatively is set for the last half of 1990.

### Universal Small Experiment Container

The wide range of carriers now available for the Space Shuttle has made payload design more difficult for the project manager. Assignment to one flight can restrict an experiment to that flight or one with comparable facilities. Reassignment may require extensive redesign in order to switch an inside payload from middeck to Spacelab, for example. In 1989 Wyle Laboratories, as a part of its participation in the CMDS, initiated design of a Universal Small Experiment Container (USEC) which would be compatible with Spacelab racks, middeck lockers, and Spacehab, and which would provide a pressure vessel for hazardous material (Fig. 2.2-3).



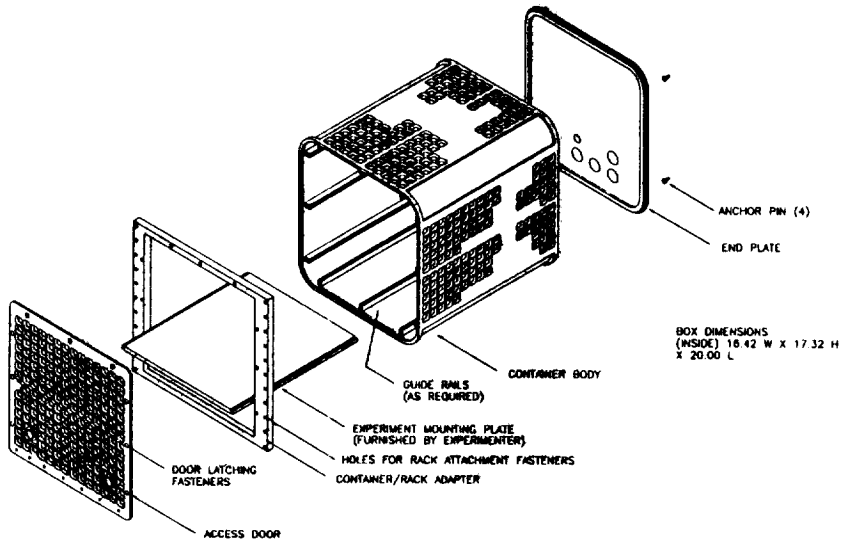


**Figure 2.2-3**
Exploded view of the proposed design for Wyle's Universal Small Experiment Carrier.

The USEC's inside dimensions (available to the experimenter) will be 43.9 cm (17.3 in.) high, 41.7 cm (16.4 in.) wide, and 49.5 cm (19.5 in.) deep. It will accommodate a total mass of 85 kg (187 lbs.) of mass for the Spacelab rack. A door will allow opening and closing in orbit and will also withstand a 20 psia pressure differential. Utility feed-throughs will be provided for four cables (two coaxial, one data, one power), and a vacuum line. Brackets inside the USEC will allow the investigators to

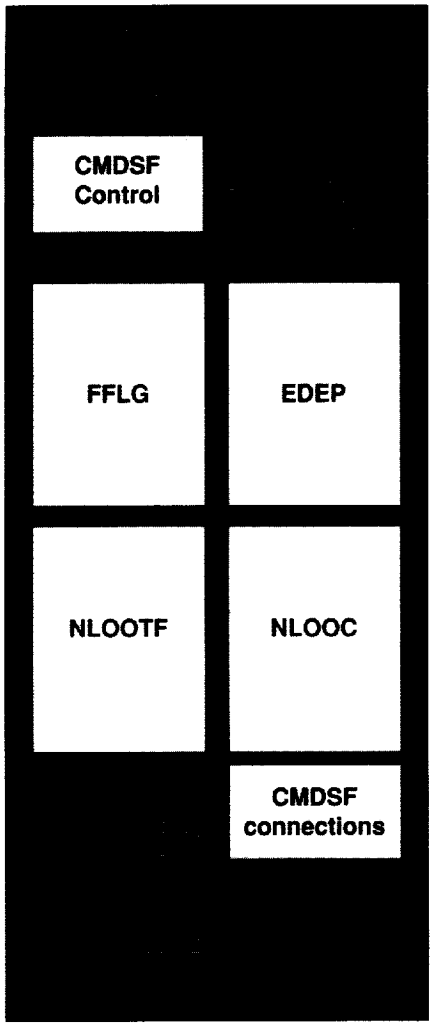


**Figure 2.2-4**
General layout of the CMDS Facility rack planned for USML-1. The payload elements are: FFLG—Formation of Foam in Low Gravity, EDEP—Electrodeposition; NLOOTF—Non-Linear Organic Optical Thin Films; NLOOC—Non-Linear Organic Optical Crystals.

insert experiment mounting plates. A flight-ready USEC will be attached by an aft mounting plate matching the mounting scheme for the Shuttle middeck lockers, or by fixtures matching the standard rack mounts on Spacelab.

Four USECs are to be flown aboard the first U.S. Microgravity Laboratory (USML-1) mission in March 1992. Another flight set is planned for the Spacehab mission, now set for September 1992. The preliminary design of the USEC was completed in the summer of 1989 and a design review was held Sept. 25, 1989. Activities planned for fiscal 1990 include the final design work and the critical design review, fabrication and testing of a qualification unit, and fabrication of the first flight unit for delivery in late 1990.

### Spacelab

A large, valuable experiment facility aboard Shuttle is Spacelab, a European-developed laboratory which fits in the Shuttle payload bay.

To make the widest possible use of Spacelab facilities that will make up USML, NASA's Office of Commercial Programs in 1988 announced that some USML-1 resources would be available to the Centers for Commercial Development of Space. As a result, a double rack aboard USML-1 will be equipped with CMDS experiments, including:

- Non-linear optical organic crystals (page 23) and thin films (page 24),
- Electrodeposition (page 17), and
- Foam formation (page 45).

The scientific investigations involved in each of these is described on the indicated pages. Much of the hardware proposed will use designs developed for the Consort 1 and GAS-105 missions described on previous pages and would be mounted in a 40-inch, double rack in the Spacelab module (Fig. 2.2-4). Although several of the experiments will be automated, USML will allow flight of a larger number of devices than a GAS can allows, and permit easier monitoring of operational parameters. Preliminary details of the experiments may be found in the 1988 CMDS annual report. These remain current with the exception of the foam formation experiment which will now be conducted by two automated devices within the CMDS Facility.

### Spacehab

Spacehab is a commercially-developed annex to the Shuttle orbiter middeck and can be outfitted with middeck lockers or Space Station-type racks. The CMDS is exploring the use of Spacehab missions to expand the flight opportunities available to it. The Spacehab 1 flight, scheduled for September 1992, is slated to carry the Boeing/CMDS Physical Vapor Transport Furnace experiment in a special rack designed for large middeck payloads. CMDS experiments aboard Spacehab will also place additional emphasis on the phase-partitioning and polymer blend experiments.

### Space Station *Freedom*

Although it is still in the advanced design phase, Space Station *Freedom* is being considered by CMDS for eventual use as an experiment facility. The permanent availability of a wide range of experiment facilities in orbit would be highly attractive.

# 3
# FLIGHT OF CONSORT 1

## Introduction

Consort 1 was the first low-g materials processing payload to be launched by a commercially licensed rocket in the United States. It carried six experiment devices which operated as planned during a seven-minute, suborbital, low-g flight and were returned in excellent condition to the investigators within four hours of launch. Nearly 150 physical samples supported by measurements and photographs made during the flight were obtained for analysis. In addition to the experimental data returned, the success of Consort 1 demonstrated the ability of industry, working with university centers and government agencies, to rapidly prepare and launch payloads.

## Flight

Consort 1, the first in a series of low-g materials processing experiment payloads sponsored by NASA's Office of Commercial Programs, was launched from the White Sands Missile Range (WSMR) in New Mexico on March 29, 1989. The general experimental objectives of the Consort 1 mission were

- Investigation of materials processing in low-g where the potential for commercial applications has been identified, and
- Development of operational concepts and flight qualified hardware for future missions using Space Shuttle facilities such as Spacelab.

This mission was the first to be accomplished under new Department of Transportation regulations for commercial space launches. Payload development, acquisition of rocket systems, systems integration, testing and launch operations were completed in approximately one year. The success of Consort 1 has been hailed as a milestone in the evolution of commercial launch services in the United States.

The launch vehicle for Consort 1 was a Starfire I vehicle furnished by Space Services Inc. of America. The Starfire is a two-stage, solid-propellant rocket with highly reliable systems for staging, telemetry, boost guidance, rate control and recovery. WSMR launch complex 36 was used for payload and rocket assembly and launch operations. The photograph on the cover of this report was taken a few seconds after first stage ignition. Debris which is visible in the rocket plume is the remains of a styrofoam box which protected the payload from exposure to low temperatures during launch countdown. The Starfire placed the payload into a ballistic trajectory providing approximately seven minutes of low gravity ($<10^{-4}$ g) with some variations due to the operation of on-board systems and rate control thruster firings.



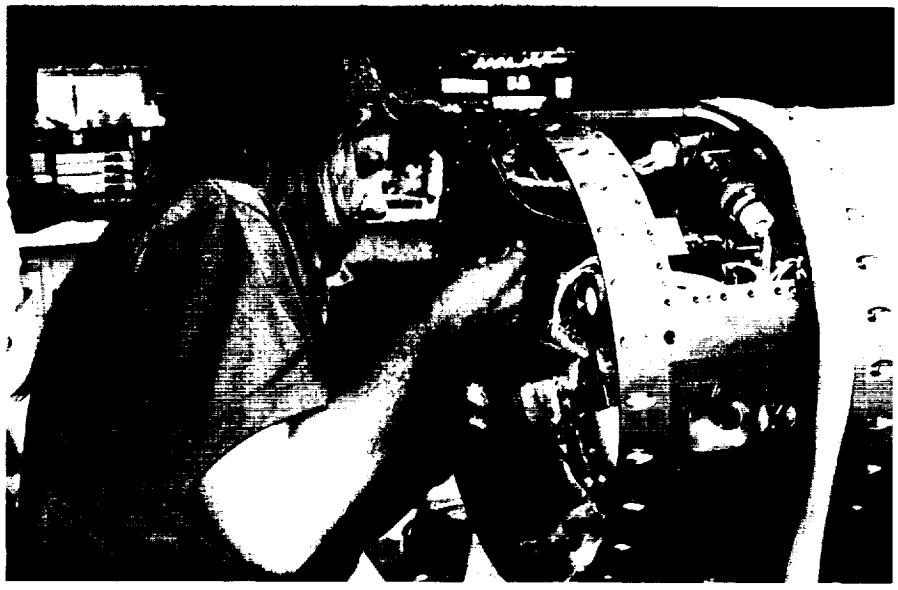

**Figure 3-1**
Anita Shelton of McDonnell Douglas works in the gas vent section of the sintering furnace apparatus.

The payload for Consort 1 was selected from among research activities under way at the CMDS. After approval of the Consort 1 flight by the CMDS and NASA, the respective investgators started developing flight hardware. In several cases they were able to adapt hardware or designs originally intended for flight aboard the KC-135, a Getaway Special, or other programs.

The payload went through several test and integration activities in

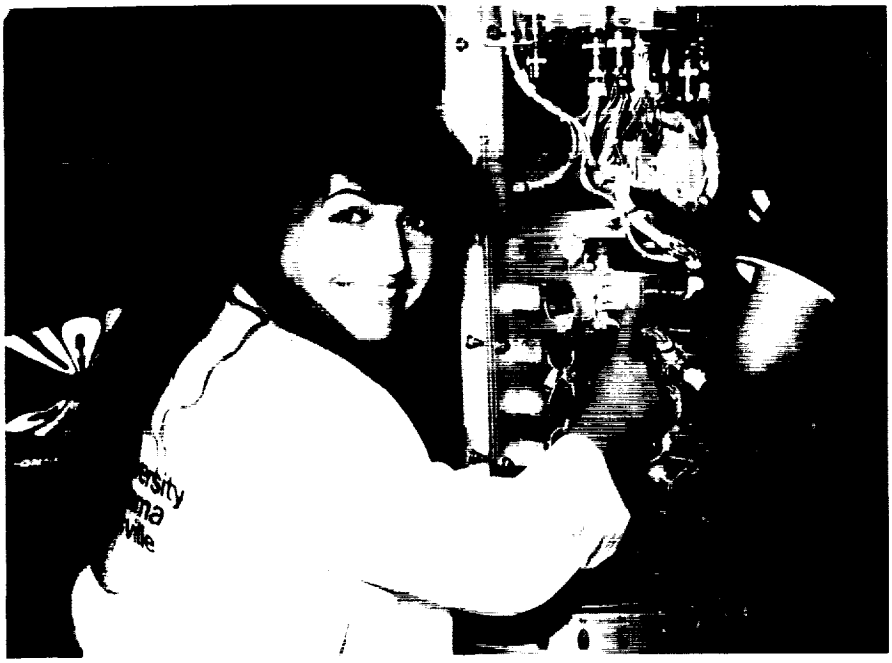

**Figure 3-2**
Hind Abi-Akar works on the electrodeposition experiment.

**Figure 3-3**
Major elements of the Consort 1 payload, as viewed from opposite sides, are depicted on page 13.

Huntsville as it was prepared for flight. McDonnell Douglas Space Systems Co., under George Maybee, supervised integration of the payload elements at UAH. Several undergraduate and graduate students were involved in this activity with MDSSC engineers. Vibration and other tests were performed at Wyle Laboratories in Huntsville. The Army Missile Command at Redstone Arsenal provided spin-balance testing which was crucial to keeping the payload stable during the low-g phase. Finally, the payload was subjected to mission sequence tests which simulated a flight from start to finish, including furnace heating cycles and onboard photography.

In early March, the Consort 1 payload was shipped to White Sands by truck. Most members of the Consort team flew in a few days later and, with the investigators, started an exhaustive set of tests which included running all the experiments through their paces and the gradual build-up of the complete payload. This led to a complete mission sequence test approximately two days before launch.

Meanwhile, SSI and its contractors were assembling the Starfire I vehicle on the launch pad about a half-mile away from the integration building. On the morning of the 28th, the completed payload and flight vehicle were brought together for the first time, and all systems were connected to instrumentation in the blockhouse. A styrofoam box was assembled around the payload to protect it from temperature extremes. In the early hours of the 29th, the completed Stafire/Consort vehicle was elevated and aimed at the sky.

The countdown proceeded smoothly and virtually without mishap. A small change in the wind caused some concern, but did not slow the pace. About a mile from the launch pad a contingent of the news media and SSI investors watched.

Finally, at T-0, the first stage of the Starfire I vehicle flashed into life and rammed the Consort 1 payload skyward. It burned out on schedule, and a few seconds later the second stage ignited for a longer burn (a few observers saw the first stage plummet back to Earth after separation). For the most part the observers only knew what they could see from the viewing site, but inside the integration building CMDS and SSI officials were watching accelerometer telemetry that showed the payload stabilize itself for the microgravity coast phase, then shudder slightly as

**Table 3-1**

**CONSORT 1 MISSION SEQUENCE**

| Event | Time (sec.) | Altitude (km MSL) | Range (km) | Velocity (m/sec) |
|---|---|---|---|---|
| **MAX Q** | **6.0** | **2.9** | **0.2** | **553.8** |
| **BBVC ignition** | **12.0** | **6.1** | **0.5** | **492.0** |
| **S-19 end of guidance** | **18.0** | **9.5** | **0.6** | **685.8** |
| Max Q/BBVC | 19.0 | 10.3 | 0.8 | 723.8 |
| BBVC burnout | 44.5 | 46.4 | 3.9 | 2217.1 |
| Yo-yo despin | 51.0 | 61.0 | 5.2 | 2116.8 |
| **Nose tip ejection** | **54.0** | **67.3** | **5.8** | **2085.8** |
| **Payload/motor separation** | **57.0** | **73.4** | **6.3** | **2061.7** |
| **Body rates nulled** | **67.0** | **93.5** | **8.4** | **1965.1** |
| Begin micro-g | 72.0 | 103.2 | 9.3 | 1916.3 |
| Apex | 281.0 | 301.2 | 49.1 | 207.9 |
| End micro-g | 491.0 | 102.0 | 86.3 | 1925.1 |
| **RCS spin-up** | **514.0** | **57.2** | **89.8** | **2134.2** |
| **S-19 power off** | **520.0** | **44.3** | **91.0** | **2180.8** |
| **Max-Q re-entry** | **538.0** | **15.9** | **93.1** | **691.3** |
| Main chute deployed | 621.0 | 4.8 | 94.2 | 96.9 |
| Landing | 861.0 | 1.5 | 93.4 | 16.5 |

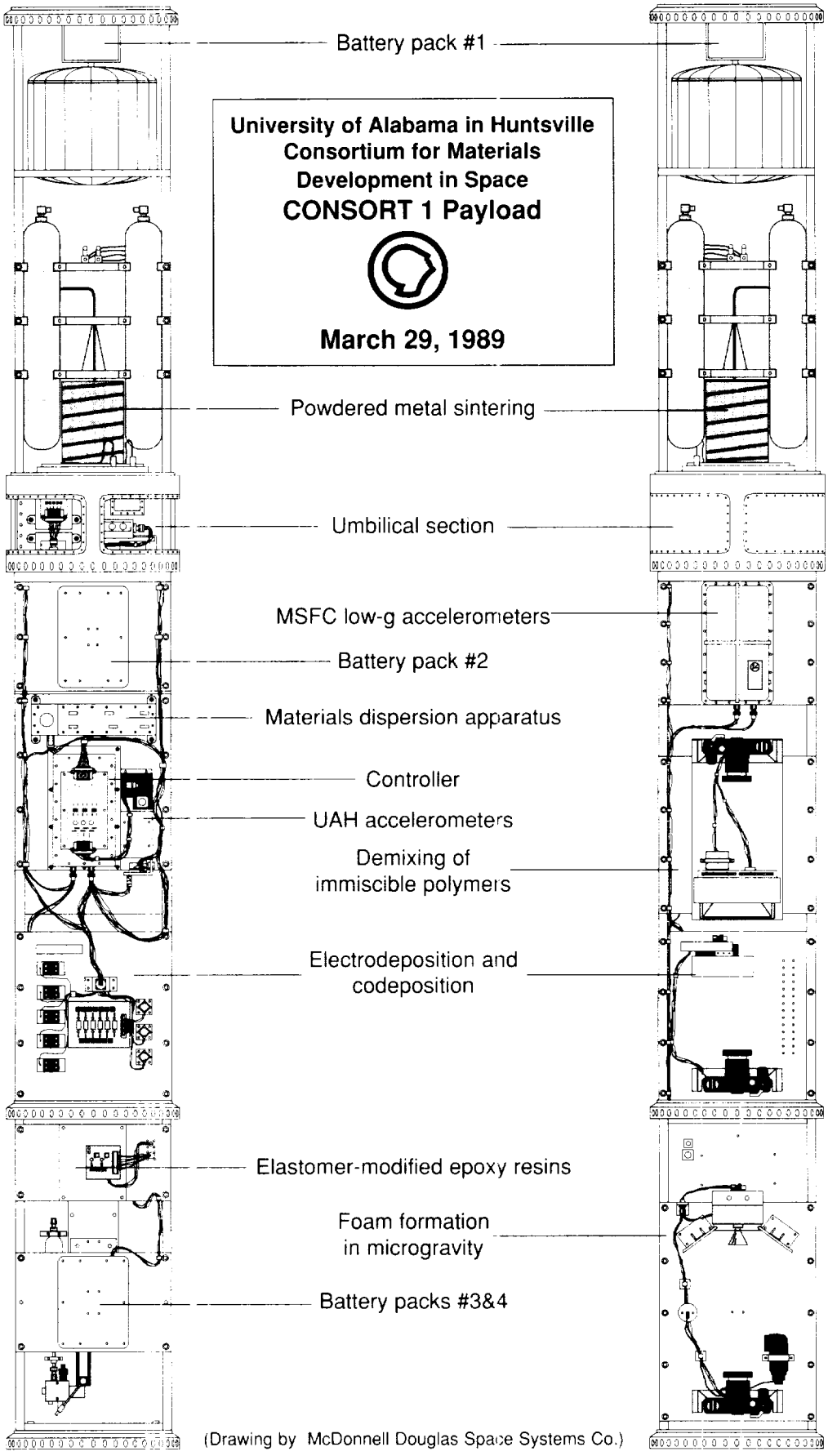


(Drawing by McDonnell Douglas Space Systems Co.)

**Figure 3-4**
All hands gather for the final stages of payload integration and test.



experiment motors and cameras did their work. Then the accelerometers went "off scale" as re-entry started and the payload plummeted back to Earth. At several miles altitude the parachutes were deployed and the payload was lowered to the desert floor. As soon as range safety confirmed that the payload was down, White Sands, CMDS and SSI teams were dispatched to recover the payload.

From launch to impact, the flight lasted approximately 14.4 minutes. Maximum velocity, reached at second stage burnout, was approximately 7,980 km/hr. Payload apex, 301 km, was reached approximately 4.7 minutes into the flight. The payload landed 93 km down range, was recovered by helicopter and a truck, and returned to the LC-36 vehicle assembly building within four hours of launch.

**Table 3-2**

**Materials Dispersion Apparatus**
**Experiment Materials**

**Biomedical Applications**
- Collagen polymerization (Bioserve Center, University of Colorado)
- Fibrin clot formation (Bioserve Center)
- Protein diffusion modeling (RANTEK Corp., University of Kentucky)
- Phenytoin precipitation (University of Arizona, NIST)
- Microtubule function (Penn State University, Center for Cell Research)

**Manufacturing Processes**
- Liquid/solid diffusion studies (Teledyne Brown Engineering)
- Ceramic and polymer membrane formation (NIST)
- Transport between immiscible fluids (NIST)

**Baseline Data for Microgravity Experimentation**
- Wetting and fluid flows in microgravity (NIST)
- Diffusion across fluid interfaces in microgravity (NIST)
- Effect of re-entry loads on materials processing products made in space (ITA, University of Wisconsin, NIST)

## Experiments

Consort 1 accommodated six experiment devices, five of which which reflect work under way at the CMDS. An overview of the preliminary results is given here; greater detail may be found elsewhere in this report.

The experiment payload was a cylinder 44 cm in diameter and 350 cm long. It weighed approximately 279 kg. Six experiments, two accelerometers, an experiment control computer and four battery packages were included in the payload. In the upper compartment, above the ground umbilical section, hardware was arranged symmetrically about the longitudinal axis. The lower compartments, which contained five of the six experiments, were divided into half-cylinders by longerons and mounting plates. This allowed experiments to be mounted in readily accessible locations on both sides of the payload centerline.

Brief descriptions of the experiments are given here; full details may be found in the individual entries that follow in this report.

**Powdered Metal Sintering:** The objective of this experiment was to examine the influences of low gravity on sintering processes using copper as the liquid-phase element and tungsten, cobalt and iron as solid-phase elements. All samples reached their desired processing temperatures (1,114°C) during the low-g period. The low-g samples were physically more uniform than the samples processed in 1-g. Their external surfaces were symmetric in appearance and they had a different hue than the 1-g reference. The same samples processed in a 1-g environment tended to be less uniform in shape with an irregular surface. The uniformity of the low-g samples at this high liquid composition was far greater than its 1-g counterpart,

which was one of the desired results

**Materials Dispersion Apparatus:** The MDA Minilab, an automated device weighing less than 2.3 kg, has the capability of using 100 to 200 samples of virtually any two or three fluids in space. The small fluid-filled cavities are aligned after the appropriate gravity condition has been established. Mixing occurs through liquid-to-liquid dispersion, with each test well accommodating fluid samples in the 50 to 400 microliter range. The apparatus was designed by ITA of Malvern, Pa. to conduct various fluid science and biotechnology experiments.

Eight principal investigators conducted a total of 11 separate investigations in the MDA (Table 3-2) during the Consort 1 sounding rocket flight, representing 103 experiment samples that were returned to Earth for subsequent analysis. The experiments were sponsored by private industry, the National Institute of Standards and Technology (NIST), and two Centers for the Commercial Development of Space. Also involved were scientists and engineers from several universities and the private sector.

**Demixing of Immiscible Polymers:** The demixing experiment apparatus included 12 cells (1.5 ml cuvettes) containing various immiscible liquids. Each cell also contained a magnetic stirring bar which could be driven by a small electric motor to mix the liquids during low-g. The apparatus operated during the low-g period as designed except that two of the cuvettes did not stir. The contents of the unstirred cuvettes separated into two phases. One phase moved to one side of the cuvette and formed an irregular shape that remained relatively unchanged and motionless during the remainder of the photographs. The seeming lack of motion was an indication of a relatively good low-g environment in the payload.

**Electrodeposition and Codeposition:** This experiment included 10 translucent electrolytic cells for investigating electrolytic processes in low-g. Key objectives were to determine the effect of deposition rate on surface morphology of nickel, obtain samples of electrically inert particles codeposited with metal, and verify results showing the production of amorphous nickel in low-g. Particle clumping experienced during codeposition on the Consort 1 flight was greater than expected. Consort 1 flight photos indicated the cermets clumped in a large mass immediately after stirring. Regardless of the clumping tendency, some codeposition was evident as shown by scanning electron microscopy photos. This indicates that either a surfactant and stirring, a surfactant and continued stirring throughout the flight, or just continued stirring may be necessary to carry out codeposition in low-g.

**Elastomer-Modified Epoxy Resins:** The apparatus contained a thin aluminum mold containing an epoxy-modified elastomer resin sandwiched between aluminum plates. Two silicon rubber heater pads were used to heat the package to 200°C and hold this temperature for five minutes during the low-g period. The objective of this experiment was to investigate the morphology and strength of elastomer-modified epoxy resins and to produce an epoxy-capped elastomer in low-g. The elastomer modified epoxy resins experiment operated as planned. Curing of the resins occurred within four minutes of reaching 200°C. The 12 samples prepared in low-g appeared translucent, which was unexpected. Electron microscopy examination of the samples is in progress.

**Foam Formation:** The objective of this experiment was to determine how the properties of polymer-gas foams are affected by preparation in low-g. It was expected that the gas bubbles would be smaller and more uniform, and that thermal conductivity and mechanical strength would be different, relative to foams formed on Earth. A gas-driven piston forced isocyanate into a chamber filled with a mixture of polyol, catalyst, surfactant and freon. The mix-

**Figure 3-5**
Wendy Bedy of the White Sands Missile Range provided the countdown.

ture was stirred for 20 seconds and then driven out of the mixing chamber through a funnel where foam formation and curing took place during low gravity. A 10- to 20-fold volume increase was anticipated during the process. After the foam was sectioned, the interior was found to be characteristic of a coarse foam. Despite its coarse appearance, one's attention is drawn to the symmetry of the cells. Coarse foams prepared in the laboratory always show more sag than equivalent compositions forming fine-celled foams.

## Discussion and conclusions

Consort 1 was an unqualified success. All six experiments returned useful data and processed materials which are under analysis for comparison with the results of ground-based experiments. The flight hardware performed according to design.

All of the payload systems, including experiment hardware, accelerometers, power packages and an experiment controller, were returned in excellent condition. Most of this equipment is slated for reflight on Consort 2 with minor modifications to improve overall performance and reliability.

The excellent data return and flight-qualification of the payload systems represents a proven capability for extended investigations on future flights.

The apparent formation of amorphous or very finely dispersed nickel by electrodeposition is a promising result. This partially verifies earlier findings reported in Europe and establishes parameters for further investigation. It is possible that the nickel sample may exhibit significantly different and beneficial properties in applications as a catalyst.

The ability of the MDA to process more than 100 samples representing a wide variety of applications was an impressive and fruitful result. The simplicity and compactness of the MDA make it an especially appropriate payload for suborbital missions.

Demixing may have occurred slower than anticipated in the 10 immiscible polymer cells which were stirred. Based on previous low-g experiments, it was expected that seven minutes would be sufficient time for demixing. This indicates that the initial condition established by stirring is a factor which must be carefully controlled to obtain consistent results in demixing processes and to enable accurate differentiation between parameters which contribute to demixing rates.

The polymer-gas foam sphere which was formed during the flight has a coarse structure, but is composed of highly spherical cells, as expected. Improvements in the mixing process are planned to enable the production of a more refined foam.

It is notable that investigators were able to service their experiments as late as 27 hours before launch and to retrieve them within four hours after launch. Late servicing and installation of experiment hardware into the rocket payload is especially important for biological experiments. While the access timing for Consort 1 was adequate, future flights will provide for some experiments to be loaded into the payload as late as three hours before launch.

The success of Consort 1 establishes a solid basis for further missions. Among the advantages offered are relatively short periods between flights (one year or less), installation and recovery of experimental packages within a few hours of launch, and seven minutes of low-g at less than $10^{-4}$ g with the capability for real-time telemetry of onboard measurements. The university-industry team which made Consort 1 possible is now moving ahead with Consort 2, scheduled for November 1989. The opportunity is open for new experiments to be included in additional missions which are planned for 1990.

**Figure 3-6**
Soon after touchdown the recovery crew was readying the payload for transport back to the integration hall.

## 4.1 SURFACE COATINGS & CATALYST PRODUCTION

**Project:** Surface coatings and catalyst production by electrodeposition and composite coatings.

**Industrial Participant:** George Maybee, McDonnell Douglas Corporation, Huntsville, AL.

**UAH Participant:** Clyde Riley, Department of Chemistry.

### Introduction

It has been reported that electrodeposition in low-g produces deposits that have differences relative to those produced in 1-g. Ehrhardt[1,2] found that nickel deposited at a high rate under low gravity (during a six-minute period aboard a British Aircraft Skylark 7 rocket) had some peculiar properties that indicated an amorphous form. This is not unreasonable since nickel has a tendency to form amorphously under high rate solidification at low temperature and when alloyed[3,4]. Likewise, electroless nickel preparation leads to a nickel containing phosphide that has characteristics of an amorphous state as defined by Tamura and Endo[5].

Since crystalline nickel is so widely used as a catalyst, its catalytic applications in near-amorphous form could be quite different. Cocke has recently reviewed the status of amorphous materials as heterogeneous catalysts, in which he highlights their advantages relative to crystalline materials. Grodzka *et al*[6] found that silver crystal deposits prepared by electrochemical displacement with copper on Skylab showed differences relative to 1-g preparations. For electrocodeposition, Ehrhardt[1,2] has reported improvements in cermet incorporation relative to 1-g. Recent electrodeposition studies by Riley *et al*[7] in the short low-g period available on a KC-135 aircraft could not duplicate the altered nickel found by Ehrhardt during low-g electrodeposition. Riley *et al*[7] also reported evidence for difficulty in suspending and dispersing neutral macroscopic particles in an aqueous medium on a KC-135. Thus, there appear to be potential applications for low-g electrodeposition, but many questions remain.

### Experiments

We prepared a flight apparatus to study electrodeposition and electrocodeposition on Consort 1 (Fig. 4.1-1). It contained 10 small electrodeposition cells: seven to deposit pure nickel, one each for codeposition of nickel/diamond dust and for a cobalt/$Cr_3C_2$ composite, and one for deposit of pure cobalt. Our major effort was directed toward the study of the effect of electrodeposition rate in low-g on the crystalline structure of deposited nickel. We also wanted to determine if neutral particles could be suspended, dispersed and codeposited in low-g.

Two methods were used to vary the electrodeposition rate. Four cells potentiostatically controlled the voltage between 4.5 and 9V at 1.5V increments. Three (at right, Fig. 4.1-1) were potentiostatically controlled at 3V, but the distance between electrodes was shortened to $^1/_4$ that of the other cells to reduce resistance. Also, in two of these three shortened cells the cathode-to-anode area ratio was decreased to $^1/_2$ and $^1/_4$ that of the last cell to give different rates. The pure cobalt was deposited at 1.5V and a pH of 4.2.

Part of the experiment apparatus was a small lightweight package which included a camera, electronics board and provisions for stirring the two codeposition cells (Fig. 4.1-2). The camera was controlled to provide pictures of the codeposition cells at approximately 15-second intervals, thus providing cermet dispersion data for the duration of the flight. Cell currents and temperature data were stored in an onboard central processor interfaced with the apparatus. Of the five electrodeposition cells, four contained nickel sul-

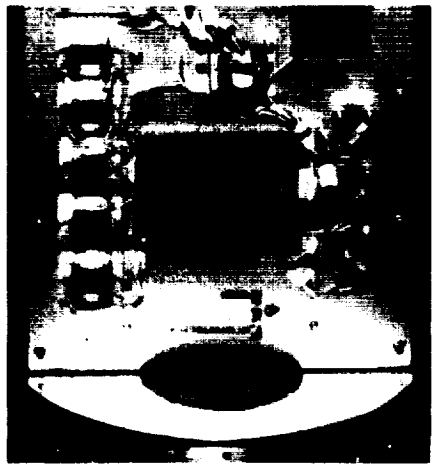

**Figure 4.1-1**
Electrodeposition apparatus, with eight cells, mounted before flight.

**Figure 4.1-2**
Codeposition apparatus was mounted opposite the electrodeposition portion.

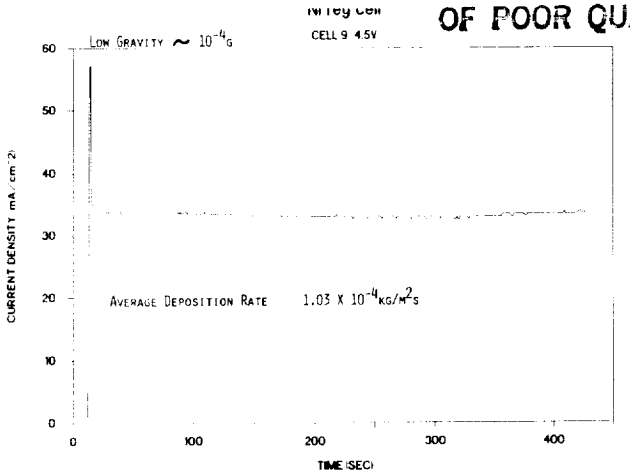


**Figure 4.1-3**
Current vs. time for the 4.5-volt nickel cell.

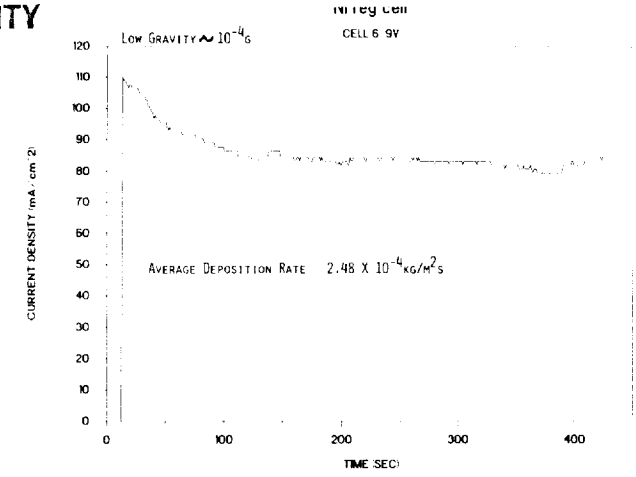


**Figure 4.1-4**
Current vs. time for the 9.0-volt nickel cell.

famate and one cobalt sulfate. These cells have been described elsewhere[8].

Several of the cells were modified to accommodate pressure changes that might accompany the high electrodeposition rates. A small channel was cut in the side of each cell's liquid holding cavity and a segment of rubber tubing sealed at one atmosphere placed in the channel. Any overpressure due to gas formation or heating compresses the tubing. These four nickel sulfamate cells deposited nickel at various rates because each was operated at a different voltage. The cobalt cell with its potential set at 1.5 volts and pH adjusted to about 4.2 was expected to deposit the B or HCP form of cobalt. The three cells on the right side of Figure 4.1-1 also contain nickel sulfamate. These are the short cells that were expected to give high currents at only 3 volts. Cathode current variation in the short cells was obtained by masking the cathode area of the second and third cells to $^1/_2$ and $^1/_4$ of that in the first cell. The electronics boards are visible at bottom center of Figure 4.1-1. The two cells mounted in the other compartment were stirred in low-g for 15 seconds and damped for 10 seconds. Undisturbed codepositon at 1.5 volts was carried out for the remaining low-g period. The computer-controlled camera took photographs before stirring, during damping and every 15 seconds into the codeposition. Illumination was provided by a backlight strobe. The stirred cells have internal stir bars, bar magnets encapsulated in glass with ridges to keep them away from the magnetic anodes (nickel and cobalt). They were turned by external 2-pole cylindrical magnets attached to the shafts of small gear motors. The magnets were turned in a cylindrical recession cut into the side of each 6-cm length cell. The codeposition particles which are of micron size can be readily viewed through the polished plexiglass cells in photographs after magnification by a factor of 10. We acquired about seven minutes of electrodeposition in low-g on the flight. The returned nickel and cobalt surfaces were analyzed by x-ray diffraction, scanning electron microscope (SEM) and X-PES.

## Results and discussion

**Nickel rate studies:** The four cells in which the rate was altered by changing the applied voltage worked well and produced interesting results. The short cells did not give the extremes in rate we had anticipated from our bench studies. The resulting surfaces produced in the short cells were identical to those found in 1-g and will not be discussed. Figures 4.1-3 and 4 show the current per unit area for two of the four regular nickel cells at different applied potentials for the low-g pe-

riod. It varies[2] from an average of ~34 ma/cm at 4.5 V to ~85 ma/cm$^2$ at 9 V. These rates bracketed that of Ehrhardt[1,2]. X-ray diffraction of the four surfaces (Fig. 4.1-5) showed a progression from the face-centered cubic (fcc) of normal nickel produced at 4.5 V to a completely x-ray transparent nickel produced at 9V. SEMs at 3000x (Figs. 4.1-6 through 9) show a steady decrease in the granularity size of the electrodeposited nickel as the electrodeposition rate is increased. X-PES (ESCA) analysis results are shown in Fig. 4.1-10. Two different spots on the 7.5 V through 9.0 V prepared surfaces were analyzed. The bars represent the atom percent of the elements detected on the surface. They are shown sequentially as *a-f* with *a* designating the 4.5 V and *f* the second 9.0 V surface (9.0 V, b). We note that carbon and oxygen are major surface contaminants. Small amounts of silicon were detected. Trace chlorine, sulfur, and calcium were also found. Copper was detected but that was to be expected since the cathodes were composed of gold-plated copper. The silicon contamination is the most worrisome and probably arises from the electroplating solution, glass storage vessels or vacuum plumbing.

Three possible explanations for these results are:

- A change in the nickel structure from face-centered cubic to amorphous,
- The formation of microcrystalline nickel that is x-ray transparent, or
- Nickel containing enough hydrogen or silicon that has resulted in an amorphous compound/alloy.

**Electrocodeposition:** The codeposition experiment was only partially successful, but it did answer some of our questions concerning suspension and dispersion of particles in low-g. We stirred for 15 seconds in low-g, damped for 10 seconds and electrocodeposited cobalt with chromium carbide or nickel with diamond dust for the remaining 400 seconds. Flight photographs showed that both types of particles had been moved but were clumped all around the sides of the cell cavities. The forces noted previously[7] apparently are strong enough to bring the particles together into large conglomerates if continued stirring is not applied. Stirring plus an additive wetting agent would be most effective, but in some cases possibly just a wetting agent alone after an initial stirring in low-g would be required. However, the latter would not prevent the generation of particle gradients during the codeposition. Scanning electron microscope images of the flight prepared codeposits at 1000x are shown in Figs. 4.1-11 and 12. Although we did not maintain good suspension/dispersion, codeposition is evident. Clumping of upwards of tens of particles is noted in the $Cr_3C_2$ with cobalt while only small groupings of several particles can be seen in the diamond with nickel.

**Temperature:** The temperature readout of the thermistor (Fig. 4.1-13) was set on plexiglass which was attached to the apparatus plate. This should give a reasonable representa-

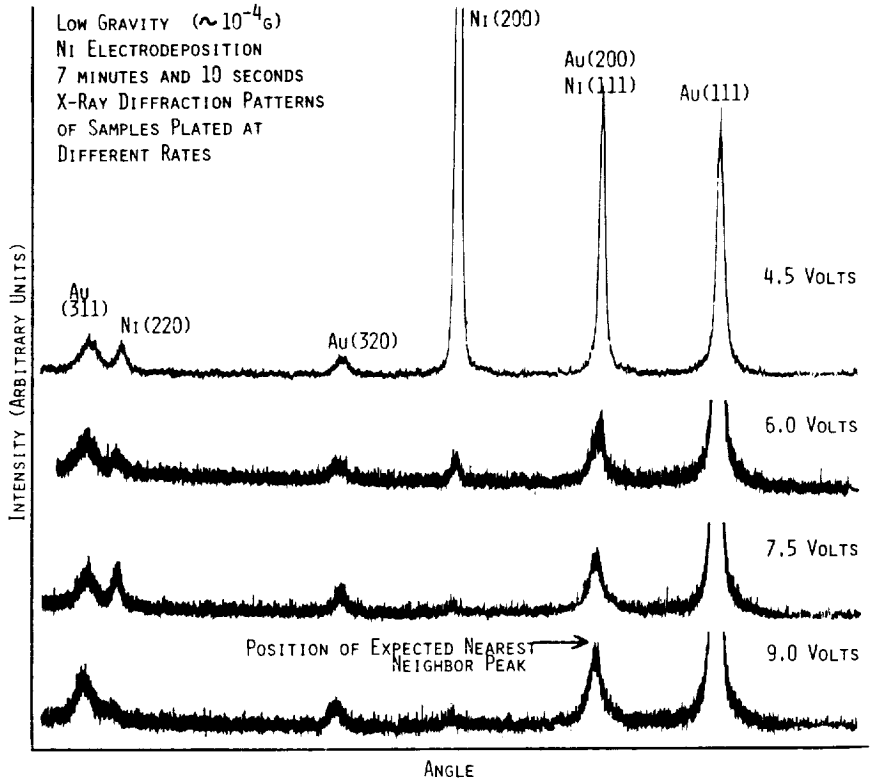


**Figure 4.1-5**
X-ray diffraction scans of the nickel surfaces.

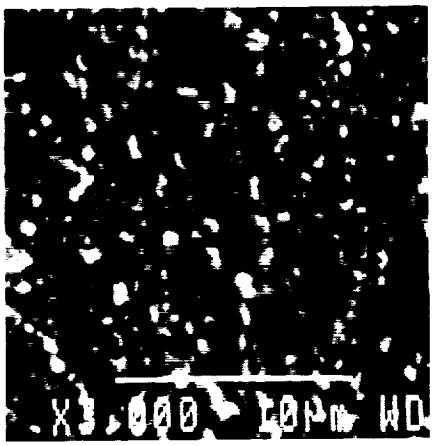


**Figure 4.1-6**
SEM of the 4.5-volt nickel surface.

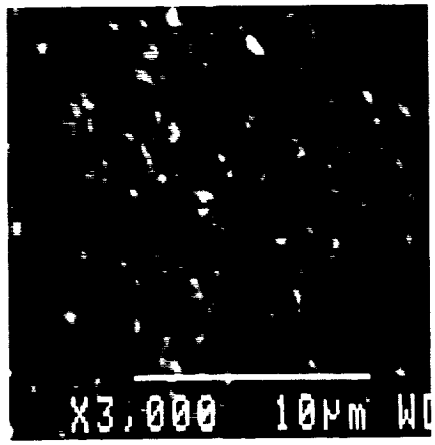


**Figure 4.1-7**
SEM of the 6.0-volt nickel surface.

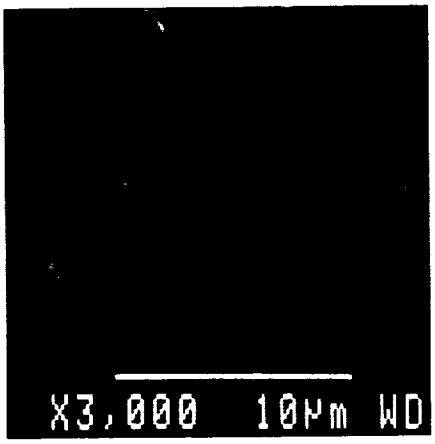


**Figure 4.1-8**
SEM of the 7.5-volt nickel surface.

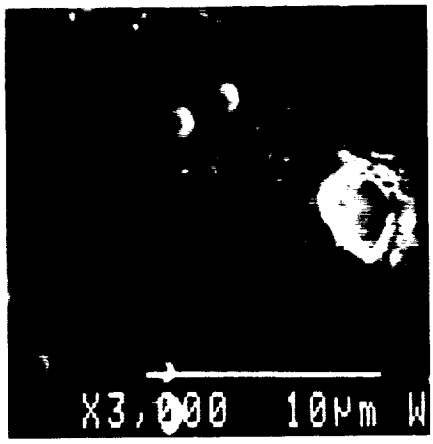


**Figure 4.1-9**
SEM of the 9.0-volt nickel surface.

**Figure 4.1-10**
X-PES surface analysis of Consort 1 samples. Units are atomic percent; values for N, Cl, S, Cu, Ca were less than 1 percent.

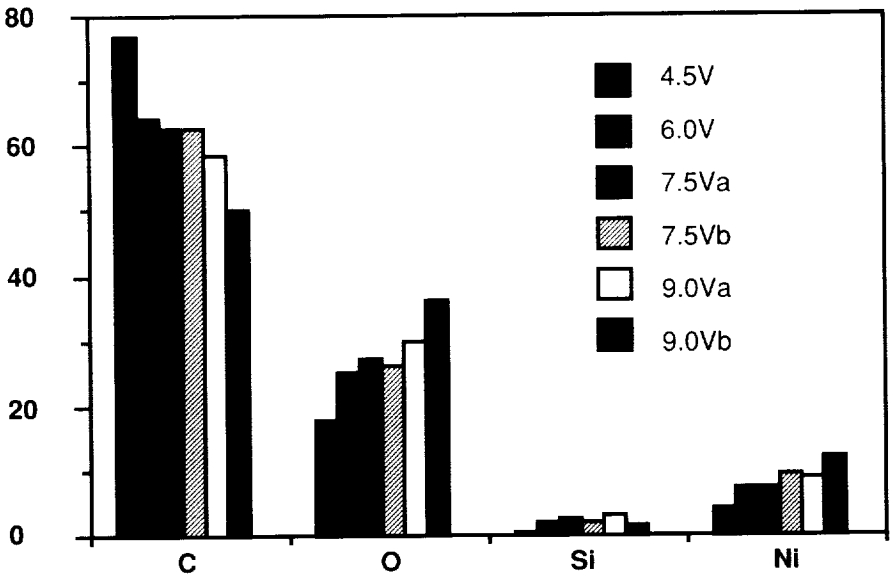


tion of cell temperature as a function of flight time. Before launch it was at 18.4°C and increased to 21.3°C during launch. During the low-g period it increased slowly from 21.3 to ~24.5°C as launch generated heat continued to be absorbed by our plate. Re-entry produced a sharp increase to more than 31°C.

## References


1. J.Ehrhardt, "Versuche zur elektrolytischem Metallabscheidung unter Schwerelosigkeit" *Galvanotechnik, D.* 7968 Sauligan 72. 13, (1981).
2. J. Ehrhardt. "Dispersion Electrolysis Under Zero Gravity Under the Spacelab Rocket Program TEXUS IV." Battelle Institute, BMFT Reference No. QV 219-AK-AN/A-ALN7910-5, April 1982.
3. ___.TEXUS VII, BMFT Reference No. 01QV219-AK- AM/A-SLN7910-5, November 1983.
4. ___. TEXUS IX, BMFT Reference No. 01 QV 014-AK/SN, November 1984.
5. H. Matsueda and B. L. Averbach, "Sputtered Films of Nickel and Nickel Oxide," *Materials Science and Engineering*, 23: 131 (1976).
6. David L. Cocke, "Heterogeneous Catalysts by Amorphous Materials," *Journal of Metals*, February, 70 (1986).
7. K. Tamura and H. Endo, "Ferromagnetic Properties of Amorphous Nickel," *Physics Letters*, 28A, 52 (1969).
8. P.G. Grodzka, B.R. Facemire, M. H. Johnston and D. W. Gates, "Electrochemical Deposition of Silver Crystals Aboard Skylab IV." *J. Crystal Growth*, 35:177, 1976.
9. C. Riley, H. Abi-Akar, B. Benson and G. Maybee, "Electrodeposition of Metals and Metal/Cermet Composites on a Suborbital Rocket," AIAA Paper 89-0308, Reno, Nevada, January 1989.
10. C. Riley, D. Coble and G. Maybee, "Electrodeposition of Metals and Metal/Cermet Compos-

ites in Low Gravity," AIAA 87-0510, Reno, Nevada, January 1987.

### Presentations and publications

1. G. Maybee, C. Riley and D. Coble, "Microgravity Effects on Electrodeposition of Metals and Metal Cermet Mixtures." Getaway Special Conference, Goddard Space Flight Center, Greenbelt, MD, October 1986.
2. C. Riley, D. Coble and G. Maybee, "Electrodeposition of Metals and Metal/Cermet Composites in Low Gravity." AIAA 87-0510, Reno, NV, January 1989.
3. B. H. Loo, C. Riley, H. D. Coble and H. Abi-Akar, "Oscillatory Behavior of Electrodeposition of Cobalt." Alabama Academy of Science meeting, Florence, AL, March 1987.
4. C. Riley, H. D. Coble, B. Loo, B. Benson, H. Abi-Akar and G. Maybee, "Electrodeposition and Codeposition Under Low Gravity/Nonconvecting Conditions." *Polymer Preprints*, 2, 470 (1987).
5. C. Riley, H. D. Coble, B. Loo, B. Benson, H. Abi-Akar and G. Maybee, "Electrodeposition and Codeposition Under Low Gravity/Nonconvecting Conditions." Invited presentation, 194th ACS National Meeting, New Orleans, LA, September 1987.
6. C. Riley, H. Abi-Akar, B. Benson and G. Maybee, "Electrodeposition of Metals and Metal/Cermet Composites on a Suborbital Rocket," AIAA 89-0308, Reno, NVa, January 1989.
7. Clyde Riley, Hind Abi-Akar, Brian Benson and George Maybee, "Electrodeposition of Metals and Composites in Low Gravity" (Submitted to *Journal of Spacecraft and Rockets*).
8. Hind Abi-Akar, Clyde Riley and George Maybee, "Electrodeposition of Metals and Electrocodeposition of Metal/Cermet Mixtures on the Consort I Sounding Rocket." 3rd Alabama Materials Conference, Huntsville, AL, September 1989.

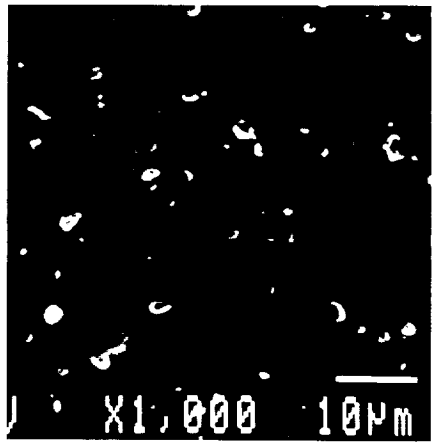


**Figure 4.1-11**
Codeposited diamond particles with nickel.


**Figure 4.1-12**
Codeposited $Cr_3C_2$ with Co.

**Figure 4.1-13**
Temperature vs. time during flight.

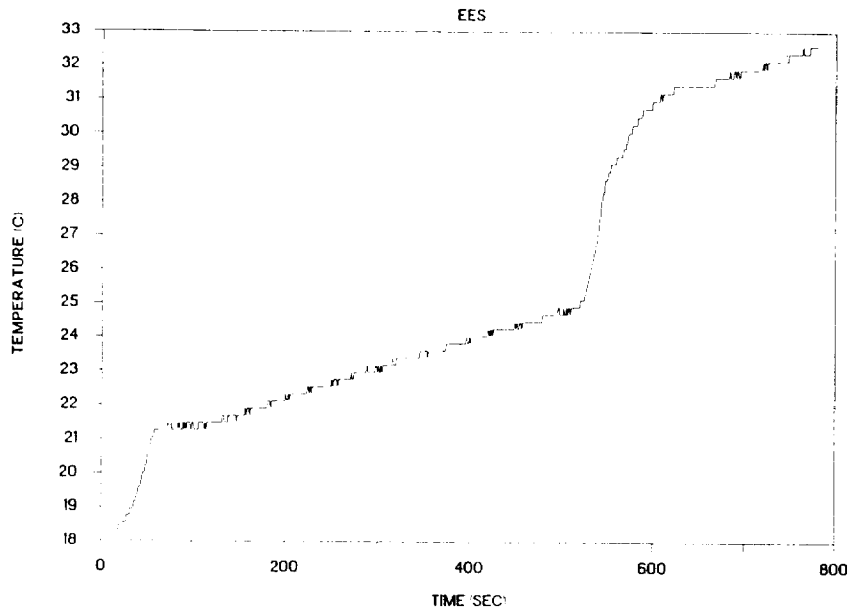

## 4.1.1 Measurement of diffusion coefficient

**Subproject:** Measurement of diffusion coefficients using the diaphragm cell

**UAH participant:** James K. Baird, Department of Chemistry

### Introduction

In our previous reports we have shown that the time, $t$, required for the solute concentration difference across the sintered glass disk in a diaphraghm cell to reach the value, $\Delta C$, was given by the infinite series in (Eq. 4.1.1-1).

Here, $B_0$ is a constant of integration which depends upon $\Delta C(0)$, the initial value of $\Delta C$, and $B_L$ and $B_1$ are given by (Eq. 4.1.1-2 through 4).

In Eq. 4.1.1-2 to 4, $D(\bar{c})$ and $D^{(1)}(\bar{c})$ are the diffusion coefficient and its first derivative, respectively, evaluated at the mean concentration, $\bar{c}$, in Eq. 4.1.1-3 where $V_1$ and $V_2$ are the solution volumes below and above the disk, while $C_1(0)$ and $C_2(0)$ are the analogous initial concentrations.

Using two diaphraghm cells with different values of $\beta$, we have collected sequences of ($\Delta C$, t) data for aqueous HCl at concentrations near 1M and fit them to Eq. 4.1.1-1 using linear regression. The values of $B_0$, $B_L$, and $B_1$ obtained with the two cells for this solution are summarized in Table 4.1.1-1. At HCl concentrations of 1M, both D(c) and $D^{(1)}(c)$ are positive. For cell 1, $V_1>V_2$; whereas for cell 2, $V_1<V_2$. Note that in each case the sign of $B_1$ given in Table 4.1.1-1 agrees with that predicted by Eq. 4.1.1-3. Knowing the geometric constants, $\beta$, for the two cells, we solved Eqs. 4.1.1-2 and 3 for $D(\bar{c})$ and $D^{(1)}(\bar{c})$ and obtained the results shown in Table 4.1.1-2. Note that the values of $D(\bar{c})$ and $D^{(1)}(\bar{c})$ obtained with the two cells are in good agreement, thus confirming our theory. By repetitions of our method for different values of C, the functional dependence of $D(\bar{c})$ (and also its slope, $D^{(1)}(\bar{c})$) can be mapped out. Knowledge of slope is useful in predicting the behavior of $D(\bar{c})$ in concentration regimes which are either too dilute or too concentrated to be tested easily in the laboratory[1].

We have used a diaphragm cell with $V_1=V_2$ to measure D(C) as a function of C for aqueous solutions of $CuSO_4$, $CoSO_4$, and $Ni(SO_3NH_2)_2$, all of which are to be used with the CMDS low-g electrodeposition experiments. Since we used a cell with volumes equal, we were assured $B_1=0$ in Eq. 4.1.1-3, and we needed to include only the first two terms on the right of Eq. 4.1.1-1 to fit our data.

A summary of the results we have obtained for these three solutions appears in Tables 4.1.1-3 through 5. The results we give for $CuSO_4$ represents an improvement on the accuracy of those reported last year. For each solution, our data cover nearly the entire solubility range of the solute. Note in each case that the diffusion coefficient decreases monotonically with increasing concentration as is the case for many salts of multicharged cations.

**Table 4.1.1-1**

**Linear regression for HCl solutions**

| | Cell No. 1 | Cell No. 2 |
|---|---|---|
| $B_0$ ($10^4$ sec.) | 8.00 | 86.8 |
| $B_L$ ($10^5$ sec.) | -1.97 | -10.8 |
| $B_1$ ($10^3$ sec./M) | -6.78 | 17.9 |

**Table 4.1.1-2**

**Differential diffusion coefficients and derivatives for HCl solutions**

| | Cell No. 1 | Cell No. 2 |
|---|---|---|
| $D(\bar{c})$ | 0.989 | 1.009 |
| $D^{(1)}(\bar{c})$ | 6.09 | 5.50 |

$D(\bar{c})$ units $10^{-5}$ cm²/sec.
$D^{(1)}(\bar{c})$ units $10^{-6}$ cm²/sec M

**Table 4.1.1-3**

**D(C) for aqueous copper sulfate at 25°C**

| C(M) | D(C) ($10^{-5}$ cm²/sec.) |
|---|---|
| 0.0188 | 0.734 |
| 0.0630 | 0.670 |
| 0.1261 | 0.565 |
| 0.2523 | 0.521 |
| 0.4539 | 0.466 |
| 0.761 | 0.426 |
| 0.964 | 0.390 |

**Table 4.1.1-4**

**D(C) for aqueous cobalt sulfate at 25°C**

| C(M) | D(C) ($10^{-5}$ cm²/sec.) |
|---|---|
| 0.020 | 0.860 |
| 0.100 | 0.720 |
| 0.300 | 0.560 |
| 0.500 | 0.479 |
| 0.700 | 0.431 |
| 0.900 | 0.401 |
| 1.40 | 0.348 |

**Table 4.1.1-5**

**D(C) for aqueous nickel sulfamate at 25°C**

| C(M) | D (C) ($10^{-5}$ cm²/sec.) |
|---|---|
| 0.02510 | 0.922 |
| 0.250 | 0.820 |
| 0.457 | 0.774 |
| 0.658 | 0.746 |
| 0.910 | 0.715 |
| 1.27 | 0.679 |
| 1.54 | 0.645 |
| 1.79 | 0.616 |

**Table 4.1.1-6**

**Equations of diffusion**

$$t=B_0 + B_L \ln(DC) + B_1(DC) + \ldots$$

$$B_L = -\frac{1}{bD(\bar{c})} \qquad \text{Eq. 4.1.1-1}$$

$$B_1 = -\frac{(V_1 - V_2)\, D^{(1)}(\bar{c})}{2b(V_1 + V_2)\,(D(\bar{c}))} \qquad \text{Eq. 4.1.1-2}$$

$$= \left(\frac{A}{L}\right)\left(\frac{1}{V_1} + \frac{1}{V_2}\right) \qquad \text{Eq. 4.1.1-3}$$

Eq. 4.1.1-4

### References


1. J.C. Clunie, *et al*, *Phys. Chem.* (in press)

## 4.2 NON-LINEAR OPTICAL ORGANIC MATERIALS

**Project:** Highly non-linear optica (NLO) crystals

**Industrial participant:** G. Bjorklund, IBM

**UAH participant:** J.M. Harris, Department of Chemistry

### Introduction

This project involves the design, synthesis, and characterization of organic materials having powerful nonlinear optical (NLO) properties (a prime example being frequency doubling), and involves the growth of crystals and films of these materials with the eventual goal of low-g growth. We are conducting research in four areas:

- Characterization of new materials,
- Synthesis of new materials,
- Techniques for choosing and preparing ordered polymer films containing NLO materials, and
- Improvement of the techniques for vapor-phase growth of high-quality organic crystals.

This knowledge will form the basis for experiments on growth of crystals in low-g.

### Characterization of new materials

We have recently developed a solvatochromic method for determining second-order polarizabilities of organic molecules for second harmonic generation (SHG)[1]. We are now working on testing the limits of this method by studying molecules which have two low-lying excited states since theory indicates this to be the most likely place for the solvatochromic approach to fail. We are also working closely with Graeme Duthie (UAH Physics Department) in setting up an optics facility for conventional characterization of NLO crystals and films.

### Synthesis of new materials

We have continued to prepare betaines for application in NLO, and we have published a paper on synthesis of a previously undescribed "ortho" betaine[2]. Recently we have completed the synthesis of an optically-active betaine. This compound is of interest because it must pack in noncentrosymmetric crystal, a property necessary for applications in NLO. Unfortunately, we have been unable to crystallize the compound, but work is continuing in this area. We have obtained another chiral betaine from C. Reichardt (Marburg University, FRG), and have begun preliminary examination of this material for use in NLO.

### Poled polymer films

The major goal of our work is to prepare crystalline NLO materials. We are, however, also working on the alternative technique of suspending NLO molecules in electrically-poled polymer films. This technique gives the alignment of the dipoles necessary for second harmonic generation. A weakness of the technique is that the aligned molecules relax to a random configuration with time. To minimize these effects we are investigating use of polyethylene glycol films in which the chains are branched and in which the NLO material (MNA) is covalently attached to the polymer. We have developed the necessary chemistry to synthesize the branched polymer and to attach NLO materials to it, and we are preparing these new films.

A major accomplishment has been our demonstration that the solvatochromic method can be used to characterize and choose polymer films for suspension of poled NLO molecules; this work is being prepared for publication and a patent application has been submitted. Solvatochromic characterization of the polymer films permits shifting (in a predictable way) of the UV-visible absorbance of the NLO material to provide resonance enhancement of the nonlinear hyperpolarizability, and to avoid absorption of the doubled frequency by the NLO material.

### Crystal growth

We continue to work closely with Franz Rosenberger of the UAH Cen-

ter for Microgravity and Materials Research and his co-workers on growth of organic NLO crystals by physical vapor transport (PVT). The PVT growth cell has gone through several modifications, and we now have an improved cell for growth up to about 200°C. New temperature baths give much better temperature control. Recent results with this cell show that we can achieve growth at one seeded spot on the the cold sting. The previous apparatus tended to give multiple nucleation sites. A modification of this apparatus will be used on our first low-g growth experiment on GAS-105 in 1990.

### Publications and presentations


1. M. S. Paley, J. M. Harris, H. Looser, J.-C. Baumert, G. C. Bjorklund, and R. J. Twieg, "A solvatochromic method for determining second-order polarizabilities of organic molecules," *J. Org. Chem.*, 54, 3774-3778 (1989).
2. M. S. Paley, E. J. Meehan, C. D. Smith, F. E. Rosenberger, S. J. Howard, and J. M. Harris, "Synthesis and properties of a novel betaine dye: 2,4- dimethyl-6-(2,4,6-triphenyl-N-pyridinio) phenolate," *J. Org. Chem.*, 54, 3432-3436 (1989).
3. J. M. Harris and M. S. Paley, "Synthesis and characterization of organic molecules for second harmonic generation," ORGN #131, ACS Meeting, Dallas, April, 1989.


## 4.2.1 Non-linear organic optical polydiacetylene thin films

**Subproject:** Polydiacetylene thin films

**Industrial participant:** Jerry Teper, Teledyne-Brown Engineering

**UAH participants:** Dr. Samuel P. McManus and Darayas Patel, Department of Chemistry

### Introduction

Some conjugated diacetylenes undergo solid-state polymerization, which may be initiated by thermal, photochemical or mechanical techniques[1-3]. The ability of a specific diacetylene monomer to polymerize in the solid-state is governed by molecular packing of the diacetylene molecules and by the nature of the substituent groups[3,4]. The polymerization proceeds through 1,4-addition and the polymer may have alternating double and triple bonds or a cumulene structure in its backbone.

Many conjugated diacetylenes undergo solid-state polymerization giving crystalline polymers with interesting conductive, mechanical and optical properties. Hence there has been a constant flow of articles describing the preparation and properties of diacetylenes[5]. The processing of these polymers, which have non-linear optical properties, interests us a great deal. Crystalline monomers have been produced by crystal growth of the monomers from solution, from melt and by the use of Langmuir-Blodgett film techniques. We have been interested in growing these monomer films by physical vapor transport (PVT) techniques[6]. PVT is considered to be the best crystal growing method for optical applications[5].

The structures of the two monomeric diacetylenes used for organic thin film growth are shown in Fig. 4.2.1-1.

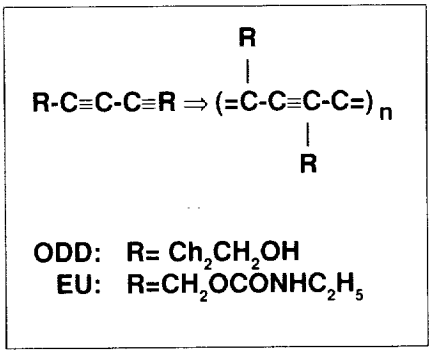


**Figure 4.2.1-1**
Schematics of two monomeric diacetylenes for organic thin film growth.

### Results and discussion

To use the PVT crystal growth technique, the choice of the substance which has sufficient vapor pressure in the desired temperature range is important. Secondly the monomer must be stable at the temperature of its use. Both of the above compounds fall into the right category for growing thin films using the PVT technique. We were successful in growing crystalline thin films of the above two monomers.

The choice of a suitable apparatus for growing good crystals by PVT is important. In our studies we have employed a Pyrex glass sublimation apparatus. We modified the apparatus for some experiments by attach-

ing a non-Pyrex glass surface. The growth apparatus was evacuated and heated to the desired temperature in the absence of the monomer. This conditioning removed any moisture or volatile impurities that may have been present on the surface. The apparatus holding the sample was heated to the required temperature using a thermostated oil bath, and was continuously evacuated using a vacuum pump.

To grow the highest quality crystals, one would like to use temperatures and pressures which would allow molecules to find their lowest energy configuration at the cooler growth surface. In the case of ODD we were not able to achieve a small difference in temperature between the condensing surface and the evaporating surface, because the melting point of the diol was low. The Experiment Unit (EU) did allow us to to achieve crystal growth with a relatively small temperature difference (8°C) between the condensing surface and the evaporating surface. In this report we will concentrate on our work with EU which is a candidate for a flight experiment.

Crystal growth of EU on Pyrex glass or polished copper plate was carried out at a reservoir temperature of 97°C and a substrate temperature between 82°C and 89°C while the pressure was maintained at 0.005 to 0.01 mm Hg. Excellent crystals were obtained with very few nucleation sites. Also the starting monomer had needle-like crystals and the microscopic photographs of the polymerized film showed fine needle-like crystals. This implies that during polymerization there is no disruption of hydrogen bonds. Several experiments on the crystal growth of the EU on polished copper plate with buffer gas argon were conducted; we were not able to see any crystal growth, probably because the condensing temperature was too high. In fact, it was near the melting point of the monomer. Also the convection current does not allow the molecule to reorient at this temperature to get organized crystal growth. We have also tried experiments where the apparatus was placed horizontally instead of vertically in the above experiments. We saw crystal growth not on the substrate but on the sides of the apparatus. Gravity plays an important role in the crystal growth but much experimental work remains before conclusions may be drawn.

An experiment to fly on USML-1 is planned for the EU. We have continued to design and fabricate hardware and the containment box. The parameters to be used for experiment control are being formulated.

### References


1. Wegner, G. Z. *Naturforsch. Teil. B.*, 1969, 24, 824-832.
2. Wegner, G. *Makromol. Chem.*, 1972, 154, 35-48.
3. Wegner, G. Chemistry and Physics of One Dimensional Metals, Keller, H.J. *Ed.*; New York: Plenum Press, 1976: p 297-314.
4. Baughman, R. H. *J. Polym. Sci. Polym. Phys.Ed.*, 1974, 12, 1511-1535.
5. Williams, D. J. Nonlinear Optical Properties of Organic and Polymeric Materials, Washington: American Chemical Society, 1983.
6. Steffen Peiser, H. Crystal Growth, New York: Pergamon Press, 1967; p 4.


## 4.2.2 Computational studies

**Subproject:** Computational study of polydiacetylenes


**UAH participants:** Samuel F. McManus, Mehdi Jalali-Heravi and Steven Zutaut, Department of Chemistry


### Introduction

One of the principle advantages of organic materials over inorganic materials in the field of optical materials is the potential for molecular engineering. Therefore, when the potential applications of diacetyle-

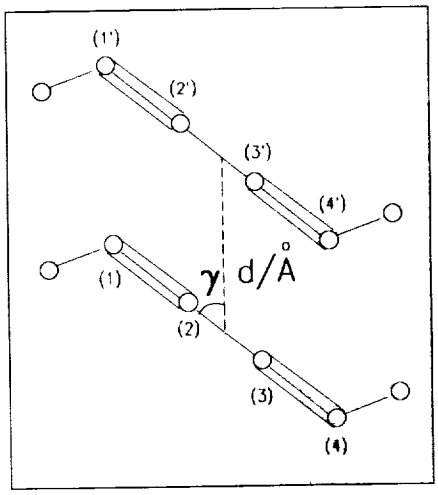


**Figure 4.2.2-1**
Schematic representation of the calculation of gas-phase packing parameters for diacetylene.

nes were recognized, laboratories around the world began synthesizing new structures which might be more readily processed. These efforts have been frustrated because no one can predict the structure and packing arrangement of molecules in a crystal. Some crystalline diacetylenes have been prepared by several groups and the crystal structures have been deduced from x-ray crystallographic studies. Those studies provide an excellent basis for comparison of theory and experiment.

We have concluded that the major problem deterring progress in the production of new diacetylene polymers with advanced optical properties, or of monomers which can be more readily processed by crystal growth methods, is the lack of good candidate materials for crystal growth studies. We are attempting to develop a methodology which will allow us to evaluate the potential of diacetylene monomers to polymerize and to provide desirable NLO properties. This method should also be applicable to other classes of NLO materials with widely varying structures in the future.

## Results and discussion

It is the goal of this study to investigate what kind of forces cause polydiacetylene monomers to align for polymerization. Secondly, it is important that we determine which substituents enhance optical properties so that we do not waste experimental efforts on polymers which have poor optical properties. We recently have begun to evaluate some available computational methods for use in predicting which diacetylene monomers should be targets for synthesis and study. Because the molecules we wanted to study are too large for practical application of *ab initio* MO methods, we turned to the best semiempirical methods currently available, the MNDO[1], AM1[2] and PM3[3] routines which are part of the MOPAC supercomputer software. We are currently running MOPAC 5.04 on the Alabama Supercomputer Network's Cray X-MP/24. We have computed several structures to determine if the results can be used to predict the behavior of structures which have not been synthesized.

Our preliminary results[4] show that polydiacetylenes with fully conjugated backbones are suitable models for theoretical investigation of the electronic properties of conjugated polymers. We have made several specific findings.

First, the MNDO, AM1 and PM3-calculated bond lengths of chlorine- and methyl-substituted polydiacetylene backbones are in good agreement with the experimental data. The calculated angles of polydiacetylene obtained using the MNDO and AM1 methods are in reasonable agreement with *ab initio* results, but one of the angles is slightly overestimated by the PM3 method.

Second, it is found that the molecular geometry of methyl- or chloro-substituted polymers fit the eneyne structure. Changing the substituents has a small effect on the bond lengths of the polymer backbone and an insignificant effect on the bond angles. The charge concentration about the carbon atom ($C_4$) (Fig. 4.2.2-1) of the backbone connecting the substituents decreases in the case of chlorine and increases by a smaller amount when a methyl group is the substituent. These changes are smaller for $C_1$ and $C_2$ which are more distant from the substituents. These results confirm that the effect of substituents rapidly diminishes as the distance from the site of substitution increases. Also, the inductive effect of a chloro group is indicated to be much stronger than that of a methyl group for short-range interactions.

Finally, for both chloro- and methyl-substituted species, the ionization potential increases as the degree of nonplanarity increases. This increment is more pronounced for methyl as compared to the chlorine-substituted polymer. As the degree of nonplanarity increases, the HOMO is more stabilized and the LUMO is more destabilized result-

ing in a blue shift in the bandgap. The overall trend variation of the bandgap as a function of an increase in nonplanarity is a red-to-blue shift. Therefore, one may conclude that the conformation of polydiacetylene backbones, with a small barrier to rotation, changes by variation of temperature. This deviation from nonplanarity will change the energies of the HOMO and LUMO and therefore the optical properties of the polymers will change.

To investigate the effect of substitution on optical properties, the bandgap of chloro- and methyl-substituted polydiacetylene monomers are compared with unsubstituted polydiacetylene. All polydiacetylenes have smaller bandgaps than the analogous monomers. Substitution for hydrogen by a chlorine atom or a methyl group changes the bandgap by at most 10 percent, while this parameter changes considerably upon polymerization. Therefore the theoretical treatment tells us that it is primarily the electronic structure of the backbone rather than that of the substituents which controls the electronic properties of the polydiacetylenes. Substituents, however, can influence the magnitude of the effect.

In a second series of SCF MO calculations just concluded[5], we have sought to find a theoretical basis for the relative reactivity of diacetylene monomers. From experimental studies of the solid-state structure of various diacetylenes, it is found that the reactivity of the monomers is somehow a function of an angle ($\gamma$) and a distance ($d$) between two monomeric units (Fig. 4.2.2-1). Obviously we would not expect a perfect correlation between the observed solid-state angles and distances (by X-ray crystallographic data) and semiempirical SCF MO calculations of gas phase molecules. Nevertheless, we have found that Dewar's AM1 program gives a remarkable plot of the angle versus the distance $d$ (Fig. 4.2.2-2). Such a plot has previously been produced from the solid-state data on known structures but it has no useful value except to show that a correlation exists.

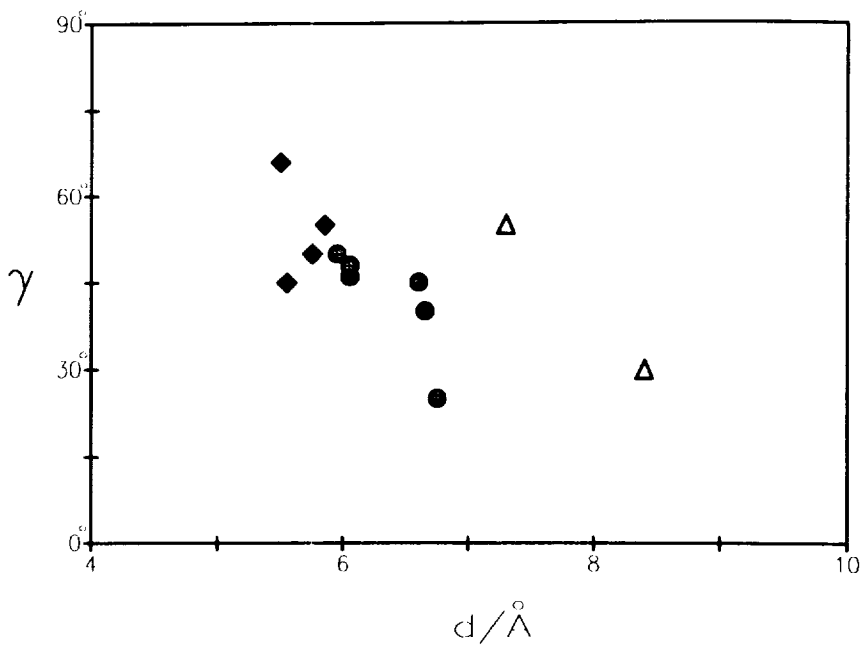


**Figure 4.2.2-2**
Plot of AM1 calculated as $d$ vs. $\gamma$.
Δ: inactive structures,
◆: reactive structures,
●: reactivity unknown.

Our plot, however, may have predictive value. For example, there is a grouping of structures known to be reactive which fall in one region on the plot and a grouping of structures known to be unreactive that fall in another region. Therefore, we would expect that unknown structures falling in either grouping may have chemical properties like those of the other members of the group.

Based on the results we have obtained using SCF MO methods, we believe that AM1 is a reliable method for the prediction of diacetylene monomer and polymer properties.

## References


1. Dewar, M. J. S. and Thiel, W. J. *J. Am. Chem. Soc.* 1977, **99**, 4899, 4970.
2. Dewar, M. J. S.; Zoebisch, E. G.; Healy, E.F. and Stewart, J. J. P. *J. Am. Chem. Soc.* 1985, **107**, 3902.
3. Stewart, J. J. P. *J. Comp. Chem.*, 1989, **10**, 221.
4. M. Jalali-Heravi, S. P. McManus, and S. E. Zutaut, *Macromolecules*, submitted for publication, 1989.
5. M. Jalali-Heravi, S. E. Zutaut, J. K. McDonald, and S. P. McManus, *Macromolecules*, in preparation, 1989.

## 4.3
## PHYSICAL PROPERTIES OF IMMISCIBLE POLYMERS

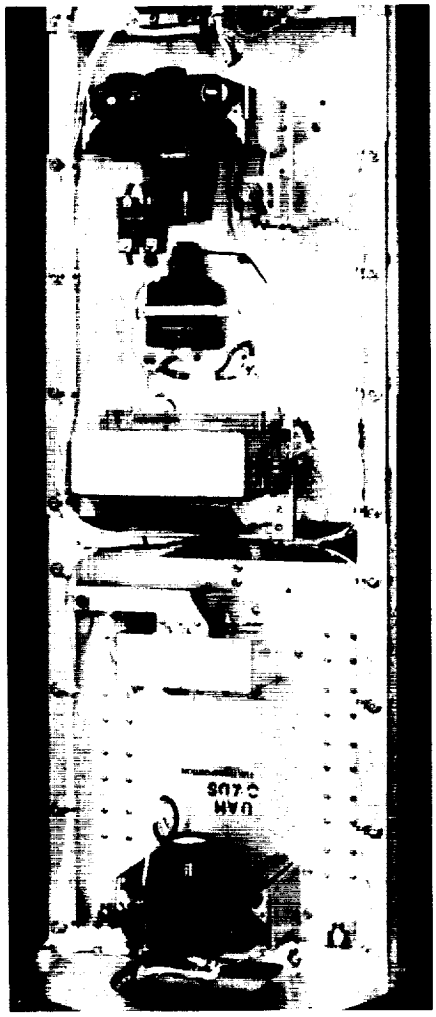

**Figure 4.3-1**
Flight hardware (at top) for demixing experiments carried out aboard Consort 1.

**Project:** Physical properties of immiscible polymers

**Indsutrial participant:** Philips Petroleum.

**UAH participant:** J. M. Harris, Department of Chemistry

### Introduction

This project is concerned with understanding and controlling the fluid physics of demixing of immiscible liquids in low-g. This knowledge will be applied to demixing of aqueous polymer two-phase systems (typically dextran, polyethylene glycol or "PEG", and water), and to use of these polymer systems to purify biological materials by partitioning between the two liquid phases. The Consort 1 flight was used to evaluate effectiveness of wall coatings to control rate of demixing and location of the two liquid phases. And a KC-135 flight was used to evaluate the effect of container shape on location of the two liquid phases. Future sounding-rocket and Space Shuttle flights will be used to further evaluate these factors. This information will then be used to assist in design and operation of a multi-step partitioning apparatus for use in population separation on the Shuttle.

Work has proceeded in four areas during the past year. These are detailed below.

### Coating control of demixing in low-g

We have previously used contact-angle measurements to show that wall coatings can be used to determine which of the two polymer phases will wet the container wall. For example, with clean glass walls, the PEG-rich phase will wet the wall and exclude the dextran-rich phase. On the other hand, dextran coatings on the glass reverse this situation and the dextran-rich phase wets the wall and excludes the PEG-rich phase; the extent to which this happens (*i.e.*, the contact angles) can be controlled by varying the molecular weight of the coatings.

In our earlier low-g experiments with clean glass containers the PEG-rich phase localized against the wall, while the dextran-rich phase was forced to the interior of the container. The first goal of a planned series of low-g flights (including the Demixing of Immiscible Phases experiment, or DIP, on Consort 1) is to test the ability of polymer coatings to control both the rate of demixing and the location of the phases. If our theories are correct, wall wetting is one of the major factors controlling the rate of demixing, and varying the contact angle of the phases with the wall should vary the rate of demixing. Also, it appears that the phase which preferentially wets the wall localizes against the wall (in low-g). Therefore, we should be able to reverse the usual egg configuration (i.e., dextran in the interior vs. PEG in the interior). By using two coatings we should have a top phase and a bottom phase, just as on Earth. This top-bottom arrangement will be important for design of the next generation of automated apparatus.

The DIP experiment was flown on Consort 1, and consisted of 12 small containers of various two-phase systems that were stirred and photographed during demixing (Fig. 4.3-1). Unfortunately, the experiment was only partially successful because of underexposure and poor development of the photographic film. The photographs are very dark and are not reproduced here. Nonetheless we could see several interesting features. First, two of our stir bars did not spin and thus the phases in these two containers were not mixed. We believe this happened because stirring was initiated before the payload entered the low-g regime (this was done to mix phases partially during the high-g period and thus minimize the amount of low-g time required to mix phases). Apparently the stir bars were not seated on the bottom of the containers, and "decoupling" of the motor and stirring bars resulted. We have reproduced this phenomenon on

Earth. As a consequence, stirring will not be initiated on the Consort 2 flight of DIP until the beginning of the low-g period.

Secondly, we observed that the phases which were mixed did not demix to any significant degree during the 7-minute low-g period, even though these same phase systems were largely demixed during this same time period on our recent STS-26 flight (PPE-2 experiment). Two possible explanations suggest themselves. First, mixing on DIP was mechanical and very efficient, whereas mixing on PPE-2 was by hand (each container held a mixing ball) and was variable and relatively inefficient. Thus it is possible that the droplet sizes obtained in DIP were significantly smaller than those obtained on PPE-2. Secondly, DIP was performed at 19°C while PPE-2 was performed at 28°C. We have previously shown that demixing proceeds more rapidly at higher temperatures.

DIP will be flown again on Consort 2. The photographic problems have been cleared up, and it is expected that this increase in photographic quality will permit us to answer the intriguing results disclosed in the first flight.

It should be noted that three groups of workers are involved in designing and interpreting the DIP experiment. They are: Milton Harris, Francis Wessling, Bruce Hovanes of UAH; Robert Snyder, James Van Alstine, Laurel Karr, and Stefan Bamberger of Marshall Space Flight Center; and Don Brooks and John Boyce of University of British Columbia.

### Shape control of low-g demixing

During the past year we have continued investigation of the effects of container shape on demixing. This work has been stimulated by the investigations of Paul Concus and co-workers (University of California at Berkeley). We recently flew an experiment with tub-shaped containers on the KC-135 (Fig. 4.3-2). These containers were filled half with water and half with air. In one case a small drop of detergent was added to the water. The water-wall contact angle was 2°. In the second case, clean water without detergent was used and the glass was coated with a commercial nonwetting silicone treatment to give a water-wall contact angle of 105°. According to the Concus theories, removal of the g-force should result in movement of fluids in the first case, but not in the second case.

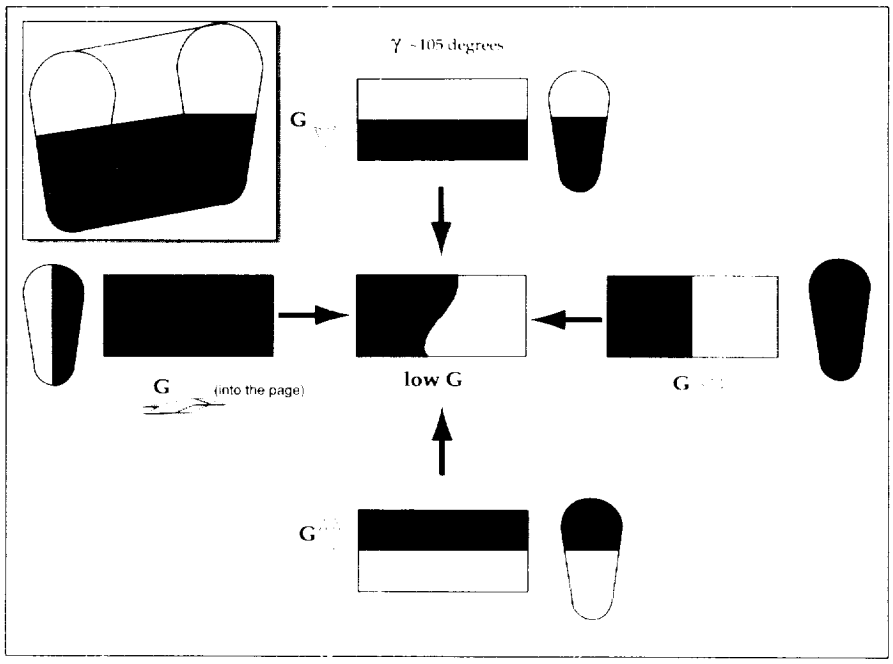


**Figure 4.3-2**
Examples of PEG wetting at 105° (above) and at 2-3° (below). Arrows with "G" indicate the preflight gravity vector on the different sample chambers, and the general shape which the sample assumed under low-g conditions.

The results of the KC-135 flight

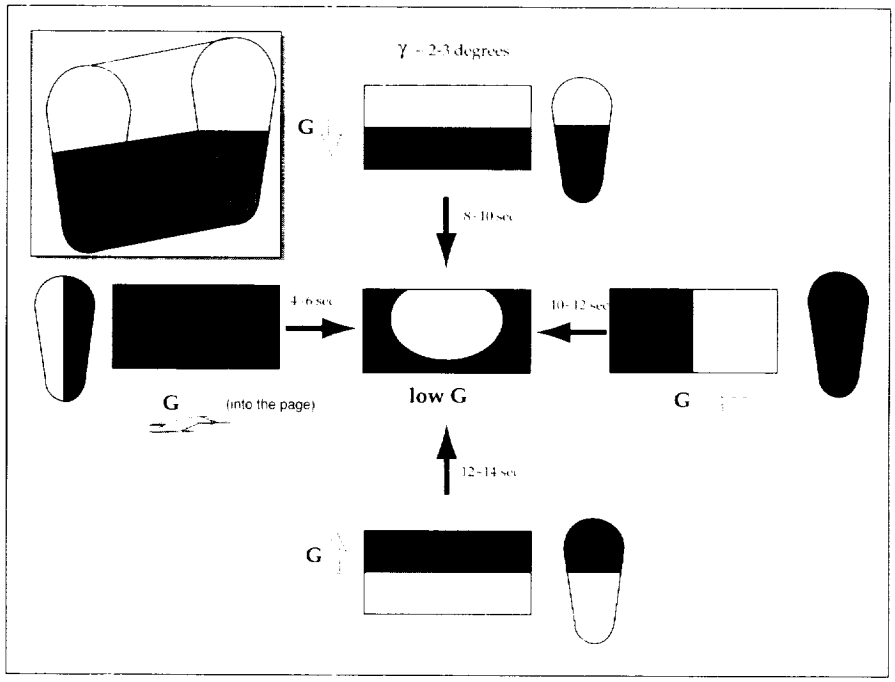

experiment with the tub-shaped containers is shown in Figure 4.3-2. Interestingly, the water did move in the first (wetting) case, to give the final configuration shown. Note that the Concus theories do not predict the final configuration. It is also interesting that in the second (non-wetting) case the fluids also move but not to the same final configuration.

Two of these same tub-shaped containers will also be flown as part of the DIP apparatus on Consort 2. In this case the containers will be filled with the aqueous polymer two-phase systems. One of the containers will be coated with dextran to give dextran wetting, while the second will be uncoated to give PEG wetting. The goal is to see if we can use container shape to control final disposition of the phases.

### Coating control of demixing at 1-g

Interestingly, we have observed that wall-wetting also affects the rate of demixing in 1-g. For example, a cuvette coated with dextran gives faster demixing that an uncoated cuvette in which the top, PEG-rich phase wets the wall. Investigations are under way to try to understand this phenomenon. The results are of use as they stand, however. Theory indicates that cell separations should proceed more efficiently in the slow demixing of a low-g environment. Thus, it is of interest to examine the effect of differing demixing rates (provided by coated and uncoated tubes) on cell separations in 1-g. Now that we have determined that this demixing-coating relationship is real, we will proceed to examine its effect on partitioning of red blood cells. This work will be done in collaboration with Laurel Karr at MSFC.

### Refinement of chemistry

The polymer coating work and the affinity partitioning procedure require a great deal of chemistry which needs improvement and extension. In the area of coating chemistry, we continue to work on optimizing the first step of attaching an active group to the surface. We now have an improved procedure for aminating glass and we have begun work on activating polymethyl methacrylate. Our recent work has been aided by the availability in the UAH Surface Science Center of an X-ray photoelectron spectrometer to analyze the aminated surfaces. In addition we have recently devised a synthesis for PEG-propionaldehye. This activated PEG appears to be of great utility for effectively modifying surfaces and proteins. Some of our previous work in this area has now been published.

### Publications and presentations


1. K. Yoshinaga and J. M. Harris, "Effects of Coupling Chemistry on Activity of a Polyethylene Glycol-Modified Enzyme," *J. Bioact. Comp. Polym.*, 1, 17-24 (1989).
2. J. M. Harris and K. Yoshinaga, "Assessment of the Effects of Tethering an Enzyme to Glass by a Polyethylene Glycol Tether," *J. Bioact. Comp. Polym.*, 4, 281-295 (1989).
3. J. M. Dust and J. M. Harris, "The picryl ether of polyethylene glycol: Preparation, characterization and reaction with n-propylamine," *J. Polym. Sci. Polym Chem. Edn.*, in press.
4. J. M. Harris, J. M. Dust, M. R. Sedaghat-Herati, R. A. McGill, and C. Upton, "New polyethylene glycols for biomedical applications," *Polymer Preprints*, 30, 356-357 (1989).
5. J. F. Boyce, B. A. Hovanes, J. M. Harris, J. M. Van Alstine, and D. E. Brooks, "The wetting behavior of aqueous two-phase polymer test systems on dextran coated glass surfaces: Effect of molecular weight," *J. Colloid and Interface Sci.*, submitted.
6. J. M. Harris, K. Yoshinaga, and J. M. Dust, "PEG derivatives for affinity partitioning," Abstracts, Third Chemical Conf., N. America, IEC #154, September, 1989.
7. R. A. McGill, J. M. Dust, M. R. Sedaghat-Herati, C. G. Upton,

and J. M. Harris, "Improved provedures for immobilization of PEG spacers onto optical fibers," ANAL #0091, ACS Meeting, Dallas, April, 1989.
8. J. M. Harris, J. E. Dust, L. J. Karr, and P. A. Harris, "New polyethylene glycols for affinity partitioning," Sixth International Conference on Partitioning in Aqueous Two-Phase Systems, Aug. 27-Sept. 1, 1989, Assmannshausen, FRG.
9. L. J. Karr, P. A. Harris, J. M. Harris, "Protein purification using immunoaffinity partitioning," Sixth International Conference on Partitioning in Aqueous Two-Phase Systems," Aug. 27-Sept. 1, 1989, Assmannshausen, FRG.
10. J. M. Van Alstine, S. Bamberger, J. M. Harris, R. S. Snyder, J. F. Boyce, D. E. Brooks, "How partitioning experiments in space improve bioseparation methods used on Earth," Sixth International Conference on Partitioning in Aqueous Two-Phase Systems, Aug. 27-Sept. 1, 1989, Assmannshausen, FRG.

**Subproject:** Elastomer-modifed epoxy resins

**Industrial Participant:** Jon Geibe, Phillips Petroleum

**UAH Participants:** J. M. Harris, Department of Chemistry, F. C. Wessling, Department of Mechanical Engineering

Our early experiments with demixing of immiscible liquids indicates that the demixing process proceeds unusually slowly in low-g to give spherical domains undistorted by sedimentation. Thus it is of interest to investigate the influence of these demixing differences on the properties of immiscible polymer blends prepared in low-g. It is reasonable to expect that domain size and morphology will affect the mechanical properties of the blends.

As a test of this concept we flew the elastomer-modified epoxy resins (EMER) experiment on the Consort I mission (Fig. 4.3.1-1). At the initiation of the experiment the resins exist as a single phase. Then heat is applied and catalytic cross-linking begins. As cross-linking proceeds, the elastomer phase separates from the epoxy phase and shortly thereafter the morphology is frozen by solidification. The goal of this experiment is to examine several of the epoxies with different compositions giving different phase-segregation points. It is expected that low-g samples will present different elastomer droplet morphologies and distributions possibly resulting in improvements in mechanical properties.

The apparatus for performing the experiment consists of a thin mold of aluminum with a series of rectangular cavities containing the resin. This mold is sandwiched by thin aluminum plates which are in turn sandwiched by two silicone-rubber heaters. The heating regime is controlled by the small computer included in the Consort payload. Mold release compound is used to prevent the elastomer-modified epoxy from adhering to the mold. A major design restriction comes from the need to heat the experiment to 200°C within two minutes and then to hold this temperature for another five minutes.

The epoxy used here consists of the bis-glycidyl ether of bis-phenol-A which has been capped with a carboxylated elastomer made of a copolymer of butadiene and acrylonitrile. We found that 1-methylimidazole is an effective catalyst for the crosslinking process since there is little crosslinking during the 72 hours at room temperature between loading the apparatus and launch. This restriction comes from the necessity to load the rocket some days before launch.

The epoxy samples obtained from the flight are still being analyzed at Phillips. Preliminary examination

**4.3.1**
**Elastomer-modifed epoxy resins**

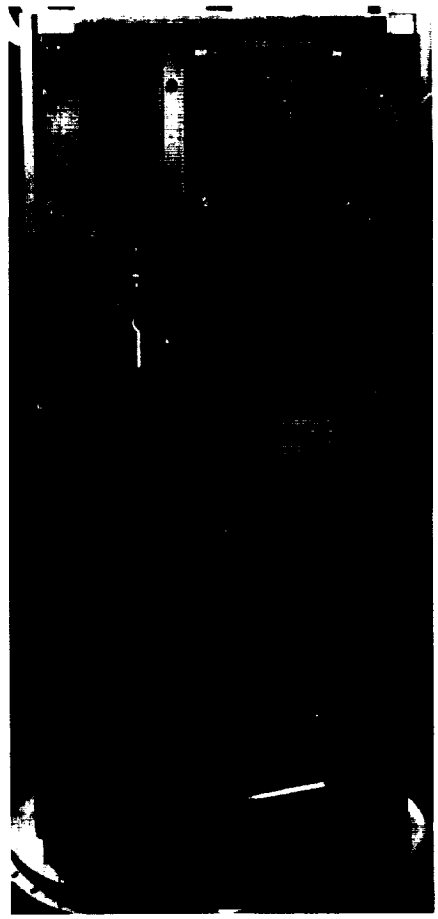

**Figure 4.3.1-1**
Flight hardware (at top) for the elastomer-modified epoxy resins experiment.

indicates that little phase segregation occurred during the flight. If phase demixing indeed proceeds more slowly in low-g (as indicated by our other work with immiscible liquids) then this would be expected. We are now attempting to develop a polymer system in which demixing occurs more rapidly so that we can more readily view the effects of gravity on these samples. The seven-minute time frame appears to be a serious restriction as longer heating at a lower temperature gives more extensive phase separation. Our new polymer system will be flown on the Consort 2 mission in November 1989.

## 4.4 NUCLEAR TRACK DETECTORS

**Project:** Nuclear track detectors

**Industrial participant:** John Gregory, Frontier Research Inc.

**UAH participants:** Samuel P. McManus, Ligia C. Christl, Chun Sheng Bu, Department of Chemistry

### Introduction

The great interest in passive particle track detectors has stimulated efforts to find better recording solids. A polycarbonate resin named CR-39 (allyl diglycol carbonate) was the result of a rational search for a plastic which is sufficiently uniform to permit the resolution of adjacent elements and perhaps even adjacent isotopes of relativistic heavy nuclei[1].

Even though CR-39 is a remarkable particle detector, it is not suitable below certain limits of ionization energy loss because of its lack of sensitivity[2]. Our preliminary studies indicate that the sensitivity can be modified by the insertion of certain functional groups into strategic locations of the basic CR-39 molecule.

In our laboratory, we have been trying to insert two methyl groups into the CR-39 monomer to obtain a more sensitive molecule. This has been done by the substitution of methyl groups at branch points of CR-39. We believe that the derivative, which we call MCR-39, diethyl glycol bis (methallyl carbonate), can be used as a monomer to make thermosetting resins for nuclear particle track detectors. After several months of work, we have obtained MCR-39. We verified its structure and purity using $^1H$ nuclear magnetic resonance and gas chromatography spectroscopy with a mass spectrometric detector.

### Conclusions

We believe that MCR-39 could replace or partially replace CR-39 as a new chemical material to make nuclear particle track detectors. These detectors made of MCR-39 homopolymer or copolymer with CR-39 could be more sensitive to cosmic rays than detectors just made of CR-39. The method we use to synthetize MCR-39 is fast and easy to follow, and has few by-products. We now have the ability to monitor each step of the synthesis. Under careful control of the temperature we can obtain a pure MCR-39 monomer. We have practiced polymerization of CR-39 and we are ready to proceed to make sample plates using copolymerization of MCR-39 and CR-39. The materials will undergo lab evaluation for sensitivity before flight testing.

### References

1. S.P. Allen, P.B. Price and G. Tarle, "Track Recording Solids," *Physics Today*, September 1981.
2. "The Chemical Design of New Nuclear Particle Track Detectors, Phase I," Frontier Research, Huntsville, AL, April 1986.

**Project:** Powdered metal sintering and infiltration

**Industrial participant:** Tripty Mookherji, Teledyne Brown Engineering

**UAH:** James E. Smith , Jr., Department of Chemical Engineering

## Introduction

This project examines the influence which low-g has on reactive liquid phase sintering of intermetallic alloys in a solid phase matrix of refractory metal.

In unit gravity, sedimentation causes stratification within the sample that results in a non-uniform coarsening of microstructure. Sintering, in a reduced gravity environment, should produce a smaller grain size, a more uniform microstructure (possibly with fewer voids or defects) and improved mechanical properties.

Potential uses for liquid-phase sintered products include bearings, magnetic materials, electrical brushes and contact points, advanced cutting tools to cut at higher linear speeds then currently possible, irregular-shaped mechanical parts for high stress environments, and possibly new and improved catalysts for chemical production.

Work during the past year has been concentrated on the development, testing, and analysis of the Consort 1 liquid-phase sintering furnace. Since the March 29 launch, work has been directed towards analysis of samples obtained during the flight and obtaining 1-g base reference samples with exactly the same operating temperatures and holding times as those used on Consort 1. In addition, we continued testing the previously built directional solidification furnace.

## Flight results

The Consort 1 liquid phase sintering furnace processed a total of nine samples with three samples from each of the following systems: copper-cobalt (Cu-Co), copper-iron (Cu-Fe), and copper-tungsten (Cu-W). Each sample used 30 percent (volume) copper. Three different copper particle sizes (149 μm [spherical], 105 μm, and 42 μm) were independently mixed with a majority phase powdered metal (43 μm Co, 6-9 μm Fe, or 1 μm W). Compacts were pressed at 11.32 tons/in$^2$ for one hour and reduced in a reactor under a flowing mixture of 5 percent hydrogen, 95 percent helium. Samples were stacked in a sample holder separated by stainless steel shims. The sample holder was installed in the sintering furnace and the Consort 1 furnace module assembled. A helium atmosphere was maintained in the furnace during operation to minimize oxidation of the samples. The sintering furnace was heated to 1040°C before launch at an approximate rate of 3.5°C/min. and held at this temperature until the beginning of low-g (L+72seconds). The furnace temperature was then increased to 1114°C at a rate of 16°C/min. to liquefy the minority phase. Total heating in low-g was 287 seconds after which began an 8-minute quench of helium to resolidify the samples and to cool the furnace ceramics to prevent sample melt-back. All samples reached their desired processing temperatures during the low-g period.

The low-g samples were physically more uniform than the samples processed in 1-g. Their external surfaces were symmetric in appearance and they have a different hue than the 1-g reference. The same samples processed in a 1-g environment tend to be much more non-uniform in shape with an irregular surface. In Figure 4.5-1a, the 6-9 μm Fe and 42 μm Cu sample, processed in 1-g, shows a rough, stressed, asymmetrical surface as compared to the symmetric, bright surface of the sample processed aboard Consort 1 (Fig. 4.5-1b). In general, powdered metal compacts processed in 1-g are restricted to a minority phase concentration of approximately 10 percent, which minimizes rearrangement and flow of the minority phase and



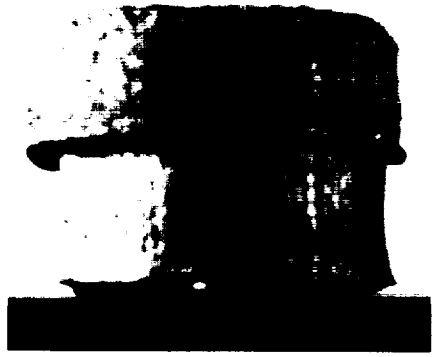

a

**Figure 4.5-1**
Photographs show 6-9 μm Fe with 142 μm Cu (top) and Fe with 42 μm Cu samples (bottom) processed in 1-g (*a*) and low-g (*b*).

b

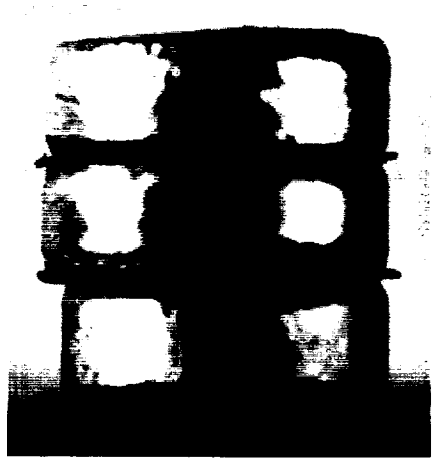

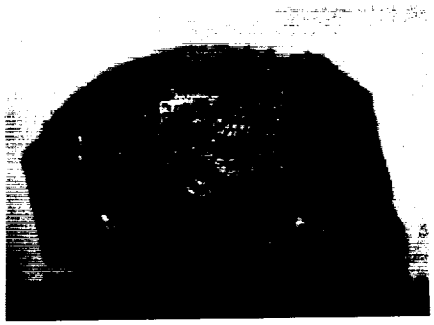

a

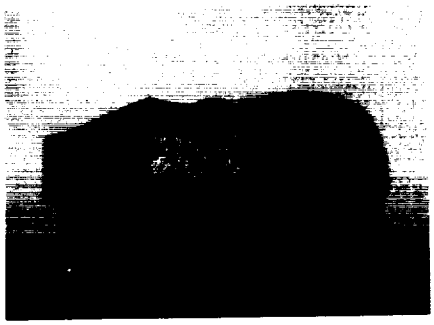

b

**Figure 4.5-2**
Photograph *a* shows two fused samples of 43 μm Co with 149 μm Cu and 105 μm Cu processed in 1-g. Photograph*b* shows 43 μm Co with 42 μm Cu sample processed in 1-g. Photographs*c-e* show: 43 μm Co with 149 μm Cu, 105 μm Cu, and 42 μm Cu samples processed aboard Consort 1.

c

d

e

produces a more uniform composite. At 30 percent liquid phase, 1-g samples are very non-uniform.

As discussed above, the uniformity of the low-g samples at this high liquid composition was far greater than its 1-g counterpart, which was one of the desired results. This is most evident in the Co-Cu systems. Figure 4.5-2 shows photographs of Co-Cu samples obtained in 1-g (a, b) and during Consort 1 (c-e). The 1-g Co-Cu samples show extreme deformation in comparison to the Consort 1 samples. It should be evident from Figure 4.5-2 that all Co-Cu samples distorted under 1-g processing, generally by wetting and flow of the liquid phase. The initially independent samples of Co with 149 μm Cu and Co with 105 μm Cu flowed to the point were they actually fused together. Careful examination of Figure 4.5-2a still shows the stainless steel shim that separated the two samples. The upper sample flowed around the shim and along the crucible wall combining to a large extent with the lower sample. The third 1-g Co-Cu sample, shown separately in Figure 4.5-2b, also shows evidence of flow within the sample and along the crucible wall. Comparison of these results and the uniform shape of the Consort 1 samples is dramatic. The Consort 1 Co-Cu samples showed no indication of flow along the crucible wall. From Figure 4.5-2, it is evident that processing of high liquid fraction Co-Cu compacts in microgravity offer performance and homogeneity not achievable in a 1-g environment.

In addition to photographic evidence discussed above, determination of sample density compared to theoretical density provides an analytical measure of the degree of densification. Average sample density was measured by weighing the samples in air and in water while theoretical density was calculated from pure component density data assuming no density changes during alloying.

The samples were weighed in a Sartorius 1702 electronic balance with .1 mg ±.05 mg accuracy. To weigh the samples in water, we constructed a basket from fine gauge stainless steel wire and suspended it from the Sartorius balance lower connection. A 2000-ml beaker filled with deionized water was positioned directly beneath the balance on a platform jack. The balance was positioned on a stable platform and the beaker positioned such that the surface of the liquid was approximately 6 inches below the balance. The basket was then submerged to a constant depth by adjusting the liquid interface with the platform jack. The balance was tared and sample placed in the basket.

The weight of sample was then recorded along with room temperature. The difference between air and water weight multiplied by the water's specific weight, at room temperature, gives the volume of the sample. Dividing air weight by volume gives the sample's average density. Green density of the pre-processed samples were determined from their weight and the volume calculated from measurements of the exterior diameter and thickness of the sample. Comparing percent theoretical density of the pre-processed sample versus final density shows that the 1-g samples differ from the low-g samples.

Percent theoretical density equals 100 multiplied by density (pre-processed or processed) divided by calculated theoretical density. The 1-g W-Cu samples showed 27, 33 and 38 percent theoretical density changes when referenced to the green state percent theoretical density for the 149 μm, 105 μm, and 42 μm Cu samples, respectively.

Comparing this to the 23, 30, and 34 percent changes for the Consort 1 samples show that the 1-g samples densify 4 percent more than low-g samples. Similar results are shown for the iron samples. These data are not available for the cobalt samples due to their condition as shown in Figure 4.5-2a.

This method was verified on pure aluminum and stainless steel

samples with known properties.

Shrinkage is another good indica tor of sintering. We recorded proc essed sample diameter divided by pre-processed diameter as percent shrinkage. The diameter was meas ured by micrometer before and afte processing. The three low-g Cu-Co samples have a measured shrinkage of approximately 9 percent, while fo the 1-g samples shrinkage was unat tainable. The low-g W-Cu samples show 1 percent swelling for the 105 µm Cu and 42 µm Cu samples and the W with 149 µm Cu sample show ing a 0.5 percent shrinkage. The W with 149 µm Cu sample is approxi mately the same for 1-g processed. The W with 105 µm sample swelled 2 percent and the W with 42 µm Cu sample shrank .7 percent in 1-g. The two larger µm Cu-Fe samples, 6-9 µm Fe with either 149 µm Cu or 105 µm Cu showed approximately 4 percent shrinkage and the remaining Cu-Fe (6-9 µm Fe with 42 µm Cu sample shrank approximately 9 per cent. The 1-g Fe-Cu samples shrank 4.7, 3.3, and 7.5 percent for the 149 µm, 105 µm, and 42 µm Cu respec tively.

## Supporting analyses

We have obtained two sets of 1-g samples using the flight furnace a conditions exactly matching those o Consort 1. Several attempts had to be made because a solid-state relay, used to control the furnace during flight, experienced a partial failure during re-entry.

To duplicate the Consort 1 mission the experiment had to be reconfig ured to emulate the flight controller using an AT computer, an external 28-volt/6-amp power supply and computer-controlled relays for event sequencing. The power distribution and timeline data from the Consort 1 mission were used as a basis for the 1-g ground control experiment. Af ter modifications and replacement o the faulty component (discussed above), two sets of samples were finally obtained under conditions which exactly duplicated the mis sion. Figure 4.5-3 shows a compari son of the temperature history ob tained during the Consort 1 mission to that finally obtained during the laboratory experiments to duplicate the mission. The temperature histo ries are nearly identical; the differ ence between heat-up time to 1040°C is due to decreased mass of the sys tem, since the 1-g experiments used only the furnace and water and he lium obtained exclusively from ex ternal sources. Additionally, the airframe above the furnace bulkhead was removed for ease of service.

The Consort 1 samples and the 1-g reference samples have been sec tioned and separately mounted for standard metallurgical analysis and surface analysis using XPS, AUGER, and SEM. The XPS analysis of the Consort 1 samples was virtually completed, with analysis of the 1-g samples about to begin. We are in the process of obtaining the chemical composition of the exterior surface of the compacts, along with distribu tions in grain size and shape of both sets of samples. The differences in

**Figure 4.5-3**
Temperature history for the Consort 1 mission and the 1-g reference experiment which sought to dupli cate the Consort results.

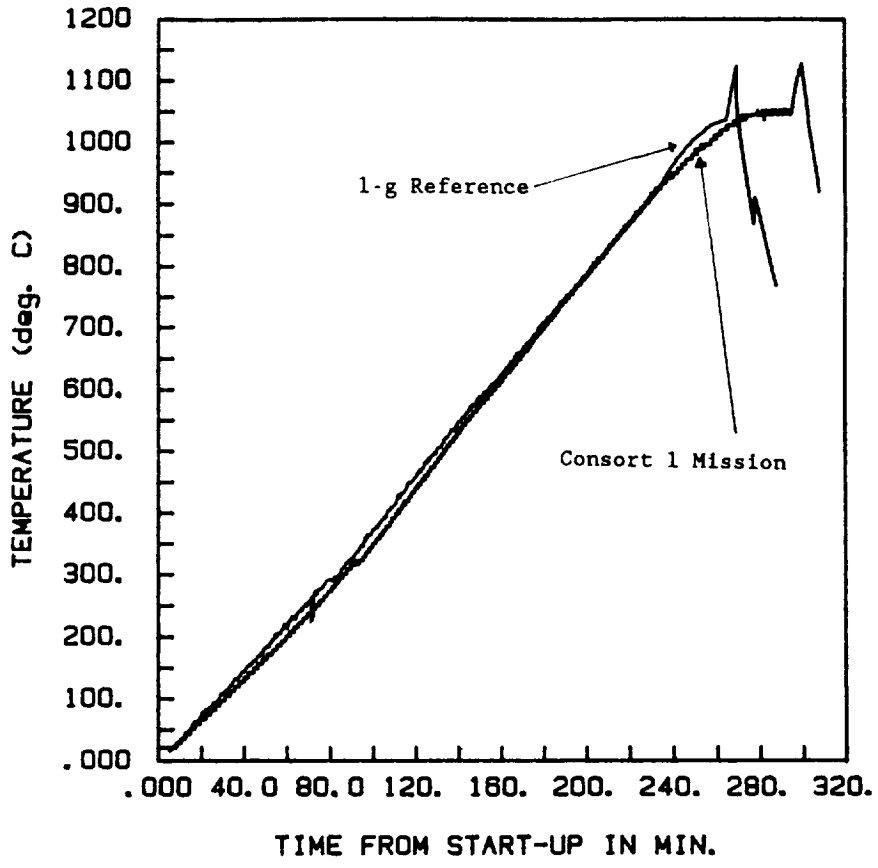

the mechanical and physical properties of the compacts prepared in low-g to that of 1-g are topics of further study.

Additionally, we have continued the performance verification of the laboratory directional solidification furnace. We directionally solidified samples in a cold over hot, and hot over cold configuration. The crucibles were stainless steel with a 6.35 mm-diameter stainless steel tube down the center line to allow temperature measurements. The experiments were performed to obtain temperature gradients along the axis of samples during directional solidification at a solidification rate of 4 mm/min. We are incorporating this data in a numerical model of the directional solidification furnace. The numerical model will help us utilize the directional solidification furnace.

### Reference


1. Smith, Jr, J.E., and Noojin, S.L., "Consort 1: Liquid Phase Sintering," 1989 Consortium for Materials Development in Space Conference, Guntersville, AL, April 19, 1989.
2. Smith, Jr, J.E., and Noojin, S.L., "An Overview of Powdered Metals Sintering Studies at UAH," Department of Chemical Engineering Seminar Series, University of Alabama, Tuscaloosa, AL, April 27, 1989.
3. Smith, Jr, J.E., and Noojin, S.L., North Alabama Chapter of SAMPE, Huntsville, AL, June 18, 1989.
4. Smith, Jr, J. E. and Wessling, F., "Engineering, Systems Integration and Preliminary Results from the Consort 1 Sounding Rocket." Department of Mechanical Engineering Seminar Series, The University of Alabama in Huntsville, AL, June 2, 1989.
5. Smith, Jr, J.E., and Noojin, S.L., "Gravitational Influences on Liquid Phase Sintering," Workshop for Commercial Flight Opportunities for Metal Alloys and High Temperature Materials Processing, The University of Alabama in Huntsville, Huntsville, AL, July 6, 1989,
6. Smith, Jr, J.E., and Noojin, S.L., "Liquid Phase Sintering Under Low Gravity Conditions," Weekly Huntsville Microgravity Seminar, Center for Microgravity Research, The University of Alabama in Huntsville, Huntsville, AL, July 12, 1989,
7. Smith, Jr, J.E., and Noojin, S.L., "Microgravity Influences on Liquid Phase Sintering," proposal to present submitted, AIChE Annual Meeting, Orlando FL, March 18-22, 1990.


## 4.6 IRON-CARBON SOLIDIFICATION

**Project:** Iron-carbon solidification


**Industrial Participant:** Norman P. Lillybeck, Deere & Co.

**UAH:** James E. Smith , Jr., Department of Chemical Engineering


### Introduction

The objective of this task is to use the microgravity environment to learn more about fundamental processes that occur in forming cast iron. This task has been held in abeyance at the request of Deere and Co. because of the lack of flight opportunities in the recent years.

## 4.7 HIGH-TEMPERATURE SUPERCONDUCTORS

**Project**: High-temperature superconductors

**Government participant**: Palmer Peters, MSFC

**National laboratory participant**: Jon Cross, Los Alamos National Laboratory

**UAH**: Elmer Anderson, John Gregory, James Ashburn, Department of Chemistry; Jan Bijvoet, CMDS

The objectives of this project are continued efforts to find high-temperature superconducting (HTSC) materials and produce them in a more useful form, and identification of HTSC devices that have commercial applications in space systems.

One of the dramatic events in the discipline occurred at UAH and was supported in part by the CMDS. On Jan. 29, 1987, M.K. Wu, James Ashburn, and their associates at UAH were the first scientists in the world to produce and measure superconductivity in a material at liquid nitrogen temperatures (77 °K). At UAH, Ashburn continues to investigate the production of crystals of the new materials and the role that the degree of oxidation plays in the characteristics of the materials. The issue of oxygen as a constituent in HTSC materials is of great importance.

Recent experiments with the Hyperthermal Atomic Oxygen Low Earth-Orbit Simulator at the Los Alamos National Laboratory have shown that oxygen-deficient films of the Perovskite yttrium barium copper oxide ($YBa_2Cu_3O_{7-x}$), HTSC materials which possess mediocre superconducting properties, were converted to high-performance HTSC materials by processing in hyperthermal atomic oxygen. The processing was performed at lower temperatures than are otherwise necessary using molecular oxygen, permitting the use of substrates such as silicon which are necessary for some devices. Normal processing of such systems results in interdiffusion and loss of performance. It appears that the high kinetic energy of the beam (1.5 electron-volts) allowed the oxygen processing to proceed at much lower temperatures.

On the ground, clean, energetic beams of atomic oxygen are difficult to produce. On the other hand, exposure to a relatively clean 5 eV beam is easily achieved in space by facing a bare specimen into the line of flight (the "windward" direction). It is planned to make such exposures for specimens supplied by a number of investigator groups. This is one of the objectives of the CONCAP 2 flight discussed previously. CONCAP 2 equipment is being prepared as a joint effort by CMDS, Marshall Space Flight Center, and Los Alamos. Samples will also be processed in flight for other organizations on a guest investigator basis. This is one example of the continuing effort to produce HTSC materials in more useful forms.

HTSC materials samples to be flown on CONCAP 2 will be half-inch squares of substrates such as quartz, strontium, titanate, silicon and gallium arsenide. HTSC films, typically of the 1-2-3 type, are deposited on these substrates by a variety of methods including sputtering and laser ablation. A subset of the thin films will have gold electrodes deposited so 4-point resistance measurements may be made. Most of the samples will operate at ambient temperature, while a selection will be maintained at an elevated temperature (300 to 320 °C) on a small hot plate.

It is still too early to foresee clearly what HTSC devices may eventually have applications in space systems. Narrowband devices are one possibility that could be valuable in communications satellites. These devices need to be perfected. The CMDS continues to play an active role in exploring and promoting the application of this technology in space.

## 4.8
## PHYSICAL VAPOR TRANSPORT CRYSTAL GROWTH

**Project:** Physical vapor transport crystal growth

**Industrial participant:** Victor Sweborg, Boeing Aerospace Co.

**UAH:** Elmer E. Anderson and Hai-Yuin Chen, Department of Chemistry

**Figure 4.8-1**
Large (1 cm x 3 mm x 2 mm) ZnSe crystal grown over a period of 11 days.

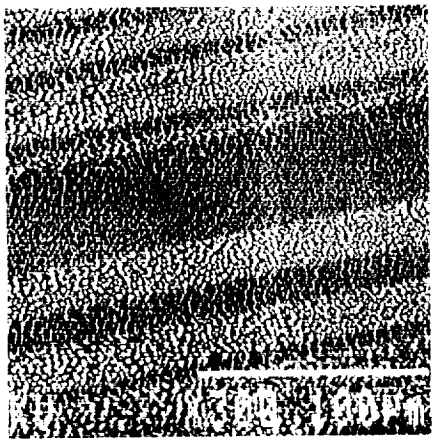

**Figure 4.8-2**
SEM picture (300x) of a {110} face after polishing and etching. The largest laminar width is about 43μm wide.

### Introduction

Single crystals of zinc selenide (ZnSe) have been grown by the physical vapor transport method in sealed quartz ampoules. The largest crystal grown measures 1 cm x 3 mm x 2 mm and required a total growing time of 11 days (Fig. 4.8-1). Polished wafers cut from the crystals have been etched and examined by optical microscopy, X-ray diffraction, scanning electron microscopy (SEM), Auger electron microscopy (AEM), and scanning Auger microscopy (SAM). No impurities or unwanted phases were detected, but extensive twinning occurred. Zinc-rich {111} faces were identified by SAM. Triangular etch pits are observed on zinc {111} faces, but not on the selenide faces. Etch pit densities are about $10^4/cm^2$ on slow-cooled samples, but are about 100 times greater when cooling is more rapid.

### Crystal growth

Our growth runs have varied in length from 9 to 32 days; a nominal yield is 2 to 6 grams of transported material. The largest average transport rate thus far is 280 mg/day. The end products of our growth runs have been of two types, either a boule approximately an inch long or a cluster of three or four faceted crystals having lengths varying from a few millimeters to about 1 cm. The shape of each boule follows the contour of the ampoule, but the boule is free of the ampoule wall. The only point of attachment is is the mouth of the acicular cavity where the growth of the boule begins. All of the samples are pale yellow in color and are clear except where regions of obvious polycrystallinity occur[1].

### Characterization

Wafers 1 to 2 mm thick were cut from boules normal to their growth directions, and crystals were cut along specific planes. The surfaces were polished with diamond paste down to a final grit size of 0.25μm and were etched in methyl alcohol for one to two minutes. The materials grown were examined for their structural homogeneity by optical microscopy, X-ray diffraction, SEM, AES, and SAM. Further details are given below.

### Growth habit

The majority of our single crystals grew in <111> directions in the form of hexagonal prisms bounded by six lateral {110} faces. This growth habit is the same as those III-V compounds which have the zincblende structure. The PVT growth rates for ZnSe vary with direction fom the highest to the lowest in the following order[2]: <100>, <111>, <110>. Therefore, one would expect the {110} faces to be predominant. However, we did obtain one small crystal with rectangular {100} faces[1].

### Twin formation

Twinning is quite evident in these materials[2,3]. Koyama *et al*[2] reported a twin density of 5 to 6/mm, with frequent 180° rotations around an axis in the <111> direction. Figures 4.8-2 and 3 show SEM photographs taken on a {110} face after polishing and etching. Note the heavy twinning in Figure 4.8-2 where the <111> growth direction is perpendicular to the bands. The largest dark band has a width of about 43μm. Figure 4.8-3 shows the same region at a magnification of 1,500 and it appears from the orientation of the etch figures that the alternating light and dark bands are due to differences in reflectivity resulting from rotations of 180° around the growth axis.

### Etch figures and etch pits

In the zincblende form of ZnSe, densely-packed planes in the <111> direction are alternately planes of

zinc atoms or planes of selenium atoms. Cleaving a ZnSe crystal perpendicular to the <111> direction will leave a zinc surface on one side and of the cut and a selenium surface on the other. It is common practice to denote them by $\{111\}_A$ and $\{111\}_B$ respectively. These planes have slightly different scattering factors and have been identified for other crystals having the zincblende structure by means of X-ray diffraction[1-6]. The stability of these surfaces has been discussed by Gatos[4] and Koyama *et al*[2]. An oxidizing etchant has been shown to produce triangular etch figures for a number of III-V and II-VI crystals[3,4]. That this is also the case for ZnSe is illustrated in Figure 4.8-4 where the triangular etch figures occur in the light-colored $\{111\}_A$ planes of zinc but not in the darker bands which are presumed to be $\{111\}_B$ planes of selenium. This is consistent with the concept that the twin bands result from 180° rotations.

Etch pits are as high as $10^6/cm^2$ for the samples that were not slow cooled. A recent run where the crystal was cooled slowly shows regions where the etch pit density is as low as $10^4$. Figure 4.8-5 is an enlarged view of a single etch pit magnified 4,000 times. Work will continue of programmed cooling rates in an effort to minimize dislocation densities.

### AES and SEM results

AES was performed using a Kratos Analytical XSAM 800 system with a 3 keV beam of electrons and a spectrometer pressure less than $10^{-10}$ torr. Only those electrons which emerge from the topmost atom layers contribute to the energy spectrum produced. For each crystal studied a survey scan was first made. This invariably showed that the predominant contaminant is carbon from exposure to the atmosphere.

After several minutes bombardment with 3 keV argon ions, the spectrum showed essentially just zinc and selenium with traces of carbon and oxygen. Upon achieving reasonable LMM line signal intensities, SAM was performed to produce chemical distribution maps of the surface of the crystal. The stripes visible across the sample from SEM imaging contain different intensities of zinc. The light lines from the SEM appear to be zinc rich, though the darker lines also contain zinc. By biasing the plotting routine to show large contrast (above 50 percent is light, below 50 percent is dark) a map is produced. Clearly the zinc is stronger in alternate lines across the sample. As was anticipated, the zinc-rich regions on these maps correspond to the zinc bands containing the etch figures in Figure 4.8-4.

The intensity of selenium, while varying from one band to another in a manner complementary to that of zinc, does not vary so strongly. A surprising result of this study is that the SAM image for oxygen shows a strong variation in concentration that is complementary to the zinc map. The SAM images produced for oxygen (same area as for zinc) show light areas that represent greater oxygen presence. In those regions where zinc is high, oxygen is lower, and vice versa. This result needs to be confirmed on other samples and the effect should be studied with other etching agents.

### Reference


1. Cheng, H.Y. and E.E. Anderson. *J. Crystal Growth* 96, 756 (1989).
2. Koyama, T., T. Yodo, and K. Yamashita, *J. Crystal Growth* 94, 1 (1986).
3. Burr. K.F, and J. Woods. *J. Crystal Growth* 9, 183 (1971).
4. Gatos, H.C. in R. Ueda and J.B. Mullin, eds., Crystal Growth and Characterization, North Holland Pub. Co., 1975, Chap. 21.
5. Warekois, E.P., and P.H. Metzger. *J. Appl. Phys.*, 30: 960 (1959).
5. Warekois, E.P., *et al. J. Appl. Phys.*, 33: 690 (1962).


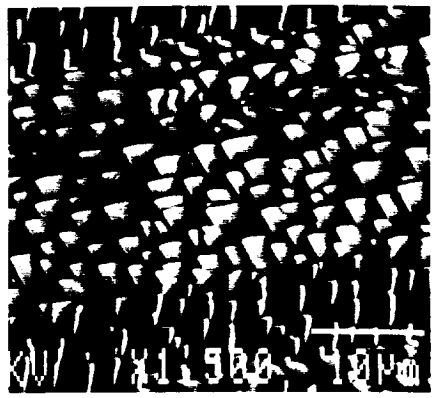

**Figure 4.8-3**
SEM picture (1500x) of the same region as Fig. 4.8-2. The orientation of the etch figures shows the rotation of the laminar twins about the growth axis. The scale bar is 10μm.

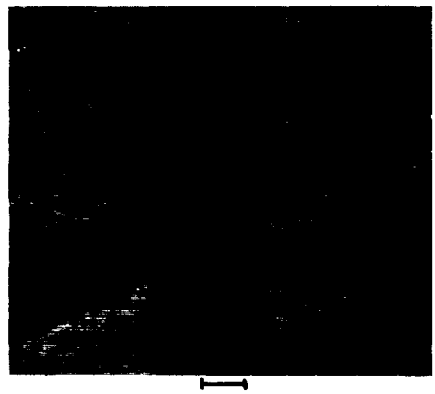

**Figure 4.8-4**
An optical photo of laminar twins. The light bands showing etch figures are $\{111\}_A$ planes. The scale bar is 20μm.

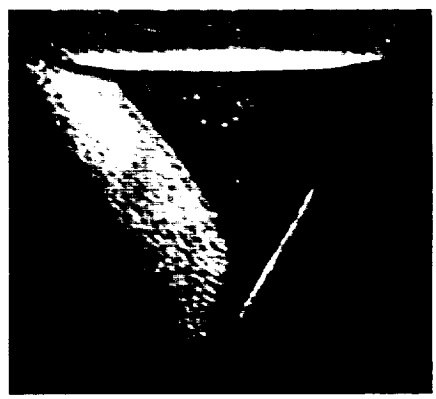

**Figure 4.8-5**
An enlarged view of an etch pit (4,000x) on a {111} surface. The pit is about 9μm on its edge.

## 4.9 MATERIALS PREPARATION AND LONGEVITY IN HYPERTHERMAL ATOMIC OXYGEN

**Project**: Materials preparation and longevity in hyperthermal atomic oxygen

**National laboratory participant**: J.B. Cross, Los Alamos National Laboratory

**UAH participants**: John Gregory and M.J. Edgell, Department of Chemistry

**Figure 4.9-1**
Carbon eroded by exposure to atomic oxygen during the STS-8 Shuttle mission illustrates the effect atomic oxygen can have on organic materials.



### Introduction and overview

A few hundred kilometers above the surface of the Earth, the most abundant constituent of the atmosphere is atomic oxygen. Formed by dissociation of molecular oxygen by ultraviolet radiation, the atoms are a major repository of solar energy in this region of the atmosphere through which low-orbit satellites pass. While the chemical reactivity of this environment has been realized for some time, only recently have observations been made of chemical and physical processes taking place involving interaction of the stream of oxygen atoms and a variety of material surfaces exposed on satellites. Since satellite velocity at typical low orbital altitudes is about 8 km/sec., much discussion has focused on the effect of this translational kinetic energy (an oxygen atom strikes a satellite surface with relative kinetic energy of 5eV) on the rates of chemical reaction. This kinetic energy is approximately equal to typical chemical bond energies, and the possibility of enhanced reaction cross-sections seems real. Fast atom fluxes in this energy range offer the possibility of surface processing in new ways, for example by production of textured surfaces with special properties or by using new channels of chemical energy opened up at these kinetic energies.

The CMDS has approached the problem in two ways: first, with a series of planned flight experiments (EOIM-3 aboard Shuttle, CONCAP-2, LDEF-A0114), and second, with laboratory work at the Los Alamos National Laboratory (LANL) orbital atomic oxygen simulation facility. In this report we discuss some results on surface chemistry of materials exposed at LANL and analyzed at UAH. We also describe the design and objectives of the CONCAP-2 Surface Reactions Experiment scheduled for flight in late 1990 (pages 8-9).

Work for the year 1989-1990 will mainly involve design, fabrication and flight of the CONCAP-2 Atomic Oxygen Experiment. Additional work at LANL is scheduled and the low energy beam facility at UAH will be completed.

### Surface chemistry studies with hyperthermal O-beams

Until recently, because of the technical difficulties of producing ample beams of oxygen atoms at several eV, few studies have been made at these energies in the laboratory and no materials chemistry experiments have been performed in space since 1983 using the source available there. While there is a wealth of data available on thermal energy ground state, $O(^3P)$, atom reaction with organic molecules, and some using atoms in the first-excited state, $O(^1D)$, very little has been reported on surface reactions, and much of that is such that it is difficult to make quantitative comparisons.

Comprehensive reviews of atomic oxygen reactions with organic compounds are available. It is now well established that the first step of the reaction of $O(^3P)$ with alkanes is abstraction of hydrogen:

$$RH + O \rightarrow R + OH,$$

though other possibilities may still occur. In the case of second and further interactions of the same residue with oxygen atoms, however, the picture is very complex and obscure. For the case of surfaces of solid polymers under consideration here, subsequent addition reactions almost certainly occur, but after each additional abstraction the possibility exists for rearrangement and loss of a volatile fragment.

Reactions with halo alkanes proceed via abstraction of available hydrogen since abstraction of a halo-

gen is too endothermic, at least in the case of thermal energy $O(^3P)$. This may not be the case for 5eV oxygen atoms, though polyfluorinated hydrocarbons are clearly less reactive in the space environment. Reaction with completely halogenated hydrocarbons may also proceed by addition mechanisms, which may be facilitated by a kinetic energy of 5eV. The massive erosion of fluorinated polyethylene observed on materials returned from the Solar Maximum Mission satellite repair was a surprise. The result has been interpreted in terms of the hydrogenated fraction of the material. The reaction rate of fully fluorinated polymers with 5eV oxygen atoms remains unquantified.

For alkenes and alkynes $O(^3P)$ adds to the unsaturated bond forming either stable products or causing rearranging and fragmenting. The relative frequency of these processes depends on the ability of the molecule to accommodate the excess energy. This ability may be high in the case of surface reactions, but the behavior with 5eV atoms is quite uninvestigated.

Reactions of $O(^3P)$ with aromatic compounds is the least well understood. Oxygen atoms may add to a carbon atom in benzene forming a radical which may rearrange to give phenol.

If a free radical remains in the surface after the first atom reaction, then reaction may occur with another atom. Since the atom arrival rate of oxygen atoms in low Earth orbit is about one per surface atom per second, the radical lifetime must be at least this long. Laboratory data on atom-radical reactions is sparse with a considerable amount of data available only for methyl radical reactions. There is, however, much published information on decomposition pathways of radicals, including those containing oxygen, and these allow deductions to be made on probable reaction paths,

$$O + R \rightarrow [RO]^* \text{ products.}$$

However, even in the case of thermal $O(^3P)$ the produced radicals are most probably excited and other pathways become energetically possible.

The situation is further complicated in the present case if 5eV kinetic energy is available. Also there is a greatly increased possibility of de-excitation of various species at the solid surface. Thus, although a good deal of data exists on reaction pathways of free radicals with oxygen atoms, the number of possibilities for reaction with polymeric surfaces is so large that elucidation of actual reaction pathways needs experimental measurement *in situ* of chemical species present on the surface, and mass spectrometric measurement of produce composition and energy. A number of general conclusions can drawn from the extensive literature on rates of reaction with $O(^3P)$. Some of these are:

- The attack of $O(^3P)$ on carbon compounds is electrophilic in nature.
- For alkanes, secondary hydrogen atoms are 10 to 20 times more likely to be abstracted than primary hydrogen atoms.
- Results for $O(^3P)$ reactions with substituted benezenes shows this electrophilic nature, with rate constants varying two orders of magnitude from $C_6H_3(CH_3)_3$ to $C_6H_5F$ and $C_6H_5CF_3$.

These conclusions are modified in the case of $O(^1D)$ reactions and may also not be valid with 5eV $O(^3P)$.

Activation energies have been measured for 5eV $O(^3P)$ reactions with solid polymer and carbon surfaces in orbit in the range of 4-7 kJ/mole. These are similar in magnitude to those observed in a variety of reactions of thermal $O(^3P)$ with organic compounds. This fact would be consistent with a model in which the rate-controlling step in the reactions of 5eV oxygen atoms with solid organic surfaces actually involved thermalized oxygen atoms bound at the surface, perhaps in a mobile precursor state. This is also consistent with a measurement of the angular distribution of 5eV oxygen atoms scattered from a carbon surface, which showed almost (but not quite)

complete energy accommodation. The present authors have also shown, however, that the absolute rate of the reaction of 5eV atoms with carbon surfaces is several times that of thermal atoms. This dependency of rate on kinetic energy only applied, according to this model, to the adsorption step of oxygen into the precursor state. The actual reaction with the organic moiety in the surface to form products may not need to consider the inclusion of 5eV of excitation energy that has already been dissipated. The following reaction sequence is postulated:

activated adsorption

$$O\ (fast) + S \rightarrow O_s^*$$

deexcitation

$$O_s + S \rightarrow O_s + S$$

re-emission

$$O_s \rightarrow O_g$$

reaction

$$O_s + RH_s \rightarrow (RHO)_s$$

$$(RHO)_s \rightarrow \text{products}$$

($_s$=surface bound; $_g$=gaseous)

**LANL RESULTS (XPS)**

| MATERIAL | CONDITION | atom% C | O | N | |
|---|---|---|---|---|---|
| KAPTON | Theoretical | 76.0 | 17.0 | 7.0 | |
| | Reference | 77.2 | 17.1 | 5.6 | |
| | Exposed | 64.1 | 28.7 | 6.2 | |
| LUCITE | Theoretical | 71.4 | 28.6 | - | |
| | Reference | 71.6 | 28.4 | - | |
| | Exposed | 66.6 | 33.3 | - | |
| CR-39 | Theoretical | 57.0 | 43.0 | - | |
| | Reference | 57.4 | 40.3 | - | |
| | Exposed | 55.4 | 39.8 | - | |
| VITREOUS CARBON | Theoretical | 100 | - | - | |
| | Reference | 81.1 | 17.6 | 1.3 | |
| | Exposed | 72.0 | 26.0 | 1.8 | |
| PYROLITIC GRAPHITE | Theoretical | 100 | - | - | FWHM |
| | Reference | 100 | - | - | (1.239) |
| | Exposed | 91.5 | 8.5 | - | (1.251) |
| POLYSTYRENE | Theoretical | 100 | - | - | |
| | Reference | 100 | - | - | |
| | Exposed | 81.3 | 18.7 | - | |

**Table 4.9-1**

## Experimental approach

Beams of fast-oxygen with kinetic energies of a few eV are now becoming available. We have initiated an experimental program at Los Alamos National Laboratory with J.B. Cross using their facility to expose solid samples of various materials at beam energies in the range 1-3eV. Extended visits to LANL were made by the principal investigator during February-March and July-August, 1989, to perform these experiments. Objectives of the work included:

- Comparison of reaction rates at carbon and polymeric surfaces of oxygen from the LANL simulator with those obtained in space at 5eV.
- Detailed surface chemical analysis using XPS of erodible surfaces exposed to the LANL beam.
- Examination of scattering profiles for oxygen atoms from carbon, gold and lithium fluoride surfaces.

Surfaces used in the XPS study of chemical reaction were: vitreous (glassy) carbon, single crystal pyrolytic graphite (basal plane), polymethylmethacrylate (Lucite), bis-allyldiglycolcarbonate (CR-39), polystyrene, and an aromatic polyimide (Kapton-H).

Material samples were typically 1 $cm^2$ in area and were cleaned with absolute ethanol before exposure. Reference samples were also cleaned in the same manner prior to XPS analysis. In the cases of the pyrolytic graphite, a clean surface was prepared in each case by cleavage using adhesive tape. Exposure conditions in the LANL beam were:

| | |
|---|---|
| flux | $2 \times 10^{16}$ atoms $cm^{-2}s^{-1}$ |
| fluence | $10^{18}$ - $10^{20}$ atoms $cm^{-2}$ |
| energy | 1.5 eV |
| substrate temp. | 25°C (nominal). |

These conditions differ from those in orbit primarily in the energy per atom (5eV in orbit). Fluences used were lower than those obtained on EOIM-2 (STS-8) since excessive erosion can produce highly roughened

surfaces, which condition may increase uncertainty in quantitative XPS. In the simplest model of erosion a steady-state composition of the oxidized surface layer would rapidly be obtained, and this would remain constant as the surface propagated through the bulk, assuming uniform composition of the bulk material. Better comparison with the reference should be obtained if the surface morphology or roughness of the exposed sample is as close as possible to that of the reference or unexposed material.

Exposures were made by placing the sample, via an airlock, in the vacuum chamber about 5 cm from the beam nozzle.

## Results

Surface analysis by XPS for the various materials is given in Table 4.9-1 in atomic percent. Theoretical values refer to the stochiometric formula of the bulk material. (For brevity, only one set of experiment results is shown).

**Kapton H**: Kapton H is a fully conjugated aromatic polyimide containing no aliphatic carbon atoms. There are two heterocyclic nitrogen atoms, four ketone groups and one ether linkage in each unit of the polymer (Fig. 4.9-2). The reference composition shows excellent agreement with the theoretical values indicating little, if any, contamination of the reference. Comparison of reference and exposed survey scans (Fig. 4.9-3) shows a clear change in the C/O ratio (4.5 to 2.2 from Table 4.9-1). The N value stays at about 6 percent, close to the theoretical 7 percent. C($^1$S) and N($^1$S) lines were examined. The components for C-O and C=O have increased with oxygen exposure, approximately from 12 to 15 percent and from 15 to 23 percent respectively. Higher chemical shifts, such as that due to carbonate, are not present. Clearly, oxygen has been inserted onto ring carbons but we cannot determine whether or not ring opening has occurred. The N($^1$S) shows broadening from 1.6 eV to 1.8eV FWHM after oxidation with ~8 percent contribution from N-O. Thus only a few of the nitrogen atoms are directly oxidized (note also that nitrogen is not preferentially removed from the surface). Broadening of the N($^1$S) peak is attributed to loss of conjugation of the molecule in the vicinity of some N atoms. This would most likely be caused by ring-opening.

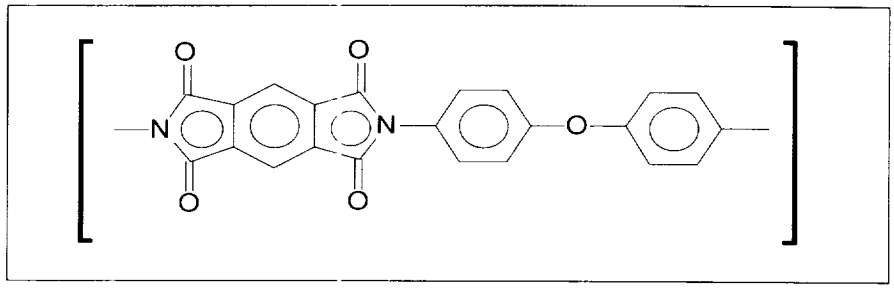


**Figure 4.9-2**
Chemical structure of Kapton H, a polymer easily eroded by atomic oxygen.

Analysis of a Kapton sample exposed several years ago on the Space Shuttle showed similar CNO percent composition data. However the fine structure is somewhat different, probably due to increased hydrocarbon contamination.

**Polymethylmethacrylate (PMMA), Lucite**: Atomic composition data by XPS show excellent agreement between the reference and theoretical values (see Table 4.9-1), while the sample exposed at LANL showed a small increased oxygen uptake (from 28 to 33 atom percent). Analysis of the C($^1$S) fine structure reveals the increase to be mainly in C=O. Since PMMA is heavily etched in this environment, chain scission must be occurring. It is plausible that the linking $CH_2$ group is attached frequently with loss of a monomer unit and formation of a residual -CHO group.

**Polystyrene**: Exposure of polystyrene to the LANL beam at 1.5eV showed large uptake of oxygen (from 4 to 19 atom percent). From this result at least 25 percent (19/81) of C atoms must be attached to oxygen after exposure. Analysis of the C($^1$S) fine structure shows 29 percent of C atoms are combined with oxygen in the ratio of 3:1 for C-O:C=O. In addition, the $\Pi \rightarrow \Pi^*$ shake-up satellite line at -7eV has been diminished

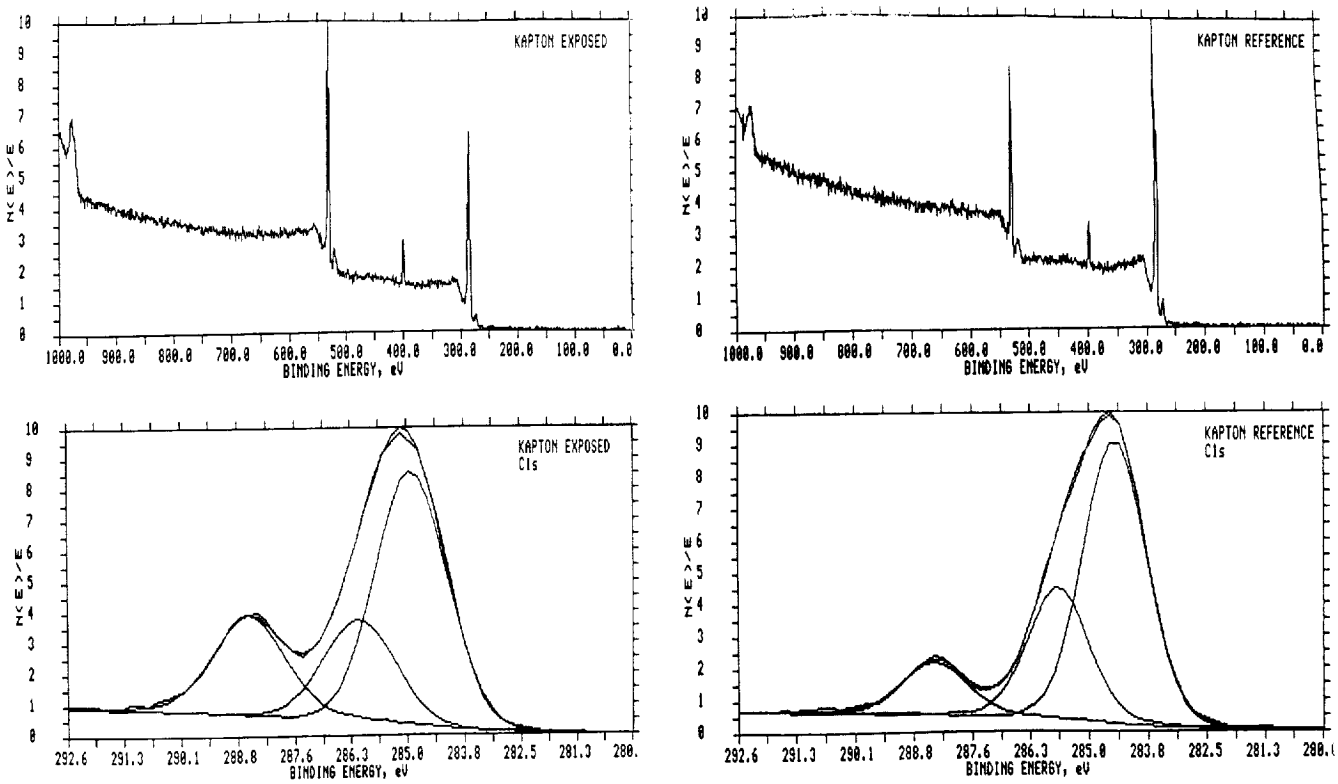


**Figure 4.9-2**
ESCA results of analyzing Kapton samples exposed to the oxygen beam at LANL. The multiple curves in the C1s graphs indicate the binding energies of carbon core electrons in different chemical environments.



showing loss of conjugation on at least some phenyl groups.

**Vitreous Carbon**: Bound oxygen increases by a small amount (8 percent) during exposure, but the reference samples show 18 atom percent oxygen before exposure. These samples are polished and cannot easily be amended. The polishing probably leaves a large number of "dangling bonds" or active sites in the surface which readily react with atmospheric oxygen. The increase is mainly in the C-O group. The nitrogen component, relatively unchanged by the exposure, is attributed to a residual from the synthetic resin used in the manufacture of this material (carbon Lorraine).

**Graphite single crystal**: The face exposed was the basal plane of single crystal pyrolytic graphite. Fresh surfaces can easily be generated by cleavage with adhesive tape. XPS analysis of these shows no impurities (including oxygen) at the 0.1 atom percentage level. Oxygen exposure showed a small (9 percent) uptake of oxygen but almost no change in the C($^1$S) peak. The $\Pi \rightarrow \Pi^*$ shake-up satellite appears relatively unaffected.

**Project:** Foam formation

**Industrial participants:** Debi Weiker, Hercules; Charlie Zusette, Thiokol

**UAH participants:** Samuel P. McManus, Department of Chemistry; Francis Wessling, Department of Mechanical Engineering; John Mathews, Darayas Patel, Department of Chemical Engineering

## 4.10 FOAM FORMATION

### Introduction

Cellular materials, formed by incorporating gas bubbles in a polymeric matrix, often have useful thermal and mechanical properties. Rigid polyurethane foams are commonly recognized as outstanding materials for insulation applications. The polyurethane molecule is prepared by the reaction (catalyzed by base or by certain transition metal salts), of a di- or polyisocyanate with a compound containing at least two hydroxyl groups. The transformation is carried out in the presence of a blowing agent, which is less soluble in the medium as the chain grows. The evolution of gas leads to a 10- to 20-fold increase in volume and, in favorable cases, a homogenous distribution of cells in the resulting foam.

A number of important structural features are required for a foam to have useful physical properties. A good foam will have cells with diameters of 200 to 1700 μm. Foams with a closed cell configuration are used for insulation and have higher mechanical strength. Foams with densities less than 0.032 g/ml cannot support a predominately closed-cell structure as the thin cell walls will rupture easily. It has been assumed that gravity influences the cell shape of a rigid polyurethane foam. Our ultimate goal is to examine the process under low-g conditions where nearly-perfect small cells may be formed. The availability of an experimental opportunity aboard the Consort 1 mission led us to initiate our program of examining the foam-forming process under microgravity conditions.

A literature survey shows that low-g experiments on metal foams have been conducted[1,2], but we were unable to locate any literature on the effects of processing at various gravity levels on the properties of polymeric foams.

In the formation of polyurethane foams the use of appropriate catalyst concentration and the choice of surfactant must be made to ensure that the medium has sufficient viscosity to hold the blowing agent. Buoyancy-driven forces will elongate cells and yield a wide range of physical properties. One may expect to have spherical cells in low-g and elongated cells at higher gravity. Our study was designed to shed light on this area.

### Result and discussion

The foam used in our studies are a formulation which includes a sucrose-based polyol from the Voranol* series and polymeric isocyanate (PAPI-94*). A 10 percent molar excess of isocyanate groups was incorporated into our mixer. DABCO 33LV* is the catalyst and the chlorofluorocarbon Genetron 11* is the blowing agent. DC 193*, a polyethylene glycol-silicon surfactant, is used to stabilize the solution of polyol, catalyst and blowing agent. Two formulations were selected for evaluation. These were designated "fast" and "slow" to indicate their relative rate of rise. The materials used are the same in both the formulations but their amounts are varied. We desired our mix to give a cream time of 15 to 40 seconds and a rise time of 100 to 225 seconds. The fast formulation has a cream time of 18 seconds and a rise time of 125 to 135 seconds while the slow formulation has a cream time of 30 to 33 seconds with a rise time of 175 to 205 seconds.

An experiment in low-g became possible with the Consort 1 flight on March 29, 1989. Our foam experiment (Fig. 4.10-1) was one of the six on Consort 1.

Our major objective was to prepare a rigid, closed-cell polyure-

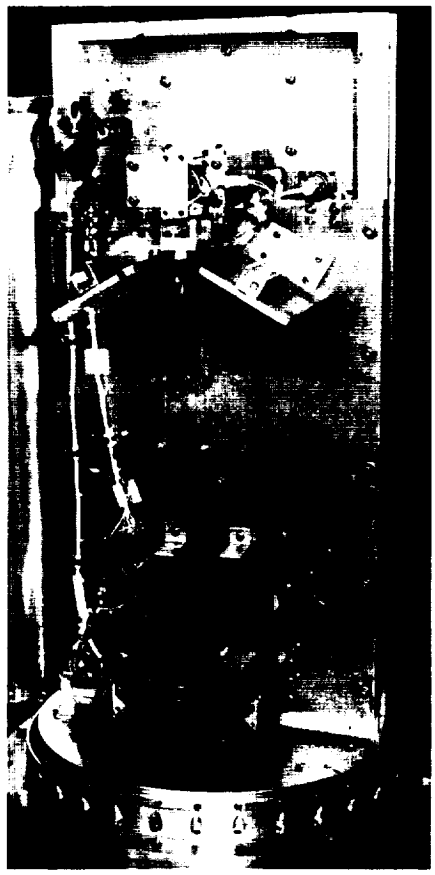

**Figure 4.10-1**
Foam formation apparatus before flight.

ORIGINAL PAGE
BLACK AND WHITE PHOTOGRAPH

**Figure 4.10-2**
Foam ball is examined after the rocket skin was removed following recovery.

thane foam with uniform cells. We used two separate piston/cylinder assemblies—one to hold the isocyanate solution (PAPI 94) and another containing a mixture of sucrose-based polyol (Voranol 360), a surfactant (DC 193), a basic catalyst (DABCO 33LV) and a blowing agent (Genetron 11). The pistons are actuated by nitrogen gas pressure. Upon reaching a preset time before low-g the isocyanate is injected into the second chamber by the piston where all the constituents are stirred mechanically for 20 seconds by a motor-driven propeller device. The mixture is then expelled through a conical exit containing a screen. A 35mm camera with flash attachments was installed in a position to capture the foaming process. Mirrors on each side of the exit funnel allow a rear view of the foam process. A thermister mounted on the exit funnel recorded the temperature profile of the experiment.

Following the successful launch of the Consort 1 payload by the Starfire I vehicle, telemetry data from the onboard accelerometer and thermister immediately revealed that the foam formation process apparently occured as programmed. Recovery of the payload occured within two hours. The payload was returned to the assembly building and dismantled revealing that foam had indeed formed on the screen as designed (Fig. 4.10-2). The foam formed nearly a symmetric ball in its confined space. Photographs taken during the flight experiment show that the process occured according to design. Photograph taken six seconds after the exit valved opened shows that no mix has exited. The photographs, taken at five-second intervals, show that the material has entirely exited after 20 seconds following the opening of the valve. Creaming is also evident in the photograph and the foaming begins at about 30 seconds. The foam rise is smooth with some surface pits because of the loss of blowing agent.

The foam sections were analyzed after sectioning. The interior of the foam was characteristic of a coarse foam as expected from a process with poor mixing. We have compared the Consort 1 foam with the two samples of foam prepared in the laboratory using an identical apparatus. In the laboratory the foam coming out of the funnel is collected in a baking pan. The interior of the 1-g foam sample is coarser and the cells are less uniform as compared to the foam made in low-g (Fig. 4.10-3). The large cells are badly deformed as compared to the low-g foam. The presence of large non uniform cells in the ground-based foam made physical property comparison of little value.

**Figure 4.10-3**
Cross-sections of foam grown in 1-G (left) and low-g (right).

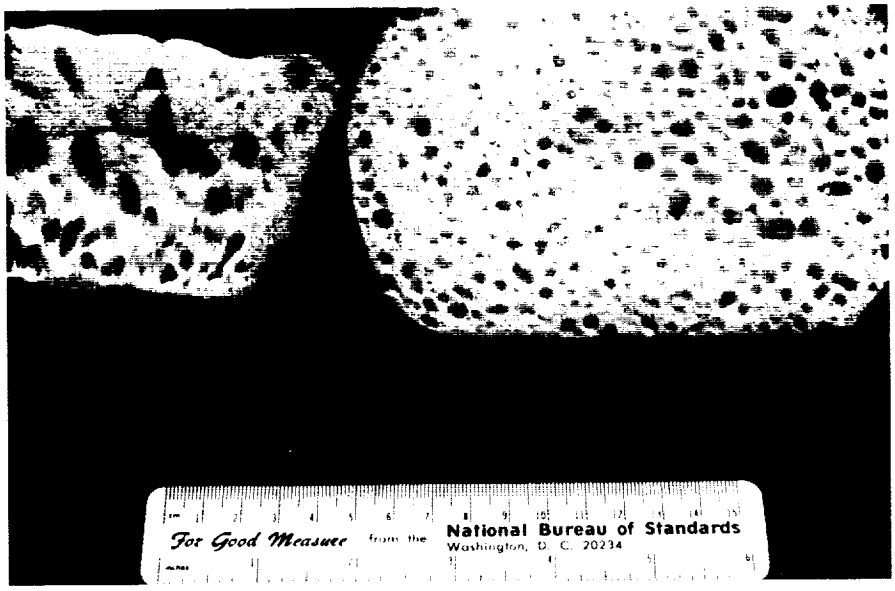


## References

1. Iliukhin, V.V. Shalimov, V. P. Budurov, S. F. Kovachev, P. D. Toncheva, S. E., "On the Conditions of Gas Inclusions Formation in Melt Under Zero Gravity State." *Acta Astronautica*, Vol. 11, 1984, pp. 595-592.
2. Patten, J. W.; Greenwell, E. N., "Feasibility of Production Closed-Cell Metal Foams in a Zero Gravity Environment from Sputter Deposition and Alloys." Post-Flight Technical Report, SPAR Flight 2, NASA CR-150178, 1976.

* ™ Dow Corp.
** ™ Allied-Signal Co.
† ™ Air Products Inc.

## 4.11 MEASUREMENT OF THE MICROGRAVITY ENVIRONMENT

**Project:** Measurement of the microgravity environment

**UAH participant:** Jan A. Bijvoet, Robert S. Newberry, CMDS

### Introduction

The aim of this activity is to develop means to measure accurately low-g disturbance levels during a payload's free-flight phase and to correlate measured quasi-steady and oscillating accelerations with rocket motions and experiment-generated disturbances. This activity also supports other CMDS projects.

Two three-dimensional accelerometers systems of different design were used: The first, the MEA Accelerometer Package or LGAS (Low-G Accelerometer System) on loan from NASA's Marshall Space Flight Center, uses three Kearfott 2412 accelerometers. Since acceleration data are integrated over one-second intervals, a high accuracy measurement of slowly varying, quasi-steady phenomena is achieved. The output noise limit is 1 x $10^{-5}$g and the bias uncertainty about 3 x $10^{-5}$g

The second, a unit assembled by the CMDS by Robert Newberry (Fig. 4.11-1), uses three QA-700 accelerometers and a triaxial mounting block from Sundstrand Data Control. Although the bias uncertainly of this system is high (8x$10^{-3}$g maximum) this system permits detection of rapidly oscillating disturbances, such as vibrations and very short pulses.

### Results

Three important results came from preflight testing and the flight itself.

First, it was decided to operate the fully assembled payload, while suspended from the ceiling of a high-bay building, and run it through a mission sequence test and record low-g disturbances. This "suspension test" turned out to be most useful: Earth's gravity could be "nulled-out" in the two axes normal to the payload/rocket central body axis down to a level of about $10^{-5}$g. The suspension method made these two axes free of disturbances. Operating the payload revealed the disturbances caused by fluid stirring motors, solenoid-actuated valves and the cameras. Subsequent bench-test investigations showed that the camera pulses were caused by the shutter and the film drive accelerations. The suspension test is also important because it allowed disturbances measured on the ground to be corellated with the measurements in flight so as to obtain a better interpretation of the in-flight phenomena.

In flight, the Consort guidance system fired rocket thrusters during low-g to compensate for a continuous yaw motion. These firings were all correlated with the measured peaks. As expected, the peaks are larger in the LGAS Y- and Z-axes which is normal for the body axes.

Second, a constant, anomalous force was detected providing a constant acceleration throughout the low-g period of 7x$10^{-5}$g in the LGAS Y-axis and 8x$10^{-5}$g in the Z-axis. In the X-axis this force is below the measurement limit (<$10^{-5}$g). The composite residual force vector was about $10^{-4}$g. This is the force as seen at the location of the accelerometer.

Figure 4.11-2 shows where the center of mass would have to be located for residual rocket roll motions to have caused the observed accel-

**Figure 4.11-1**
Robert Newberry of UAH finishes installation of an accelerometer package.

**Figure 4.11-2**
Accelerometer measurements in the X axis is typical of LGAS measurements during the flight. Arrows at bottom indicate thruster firings.

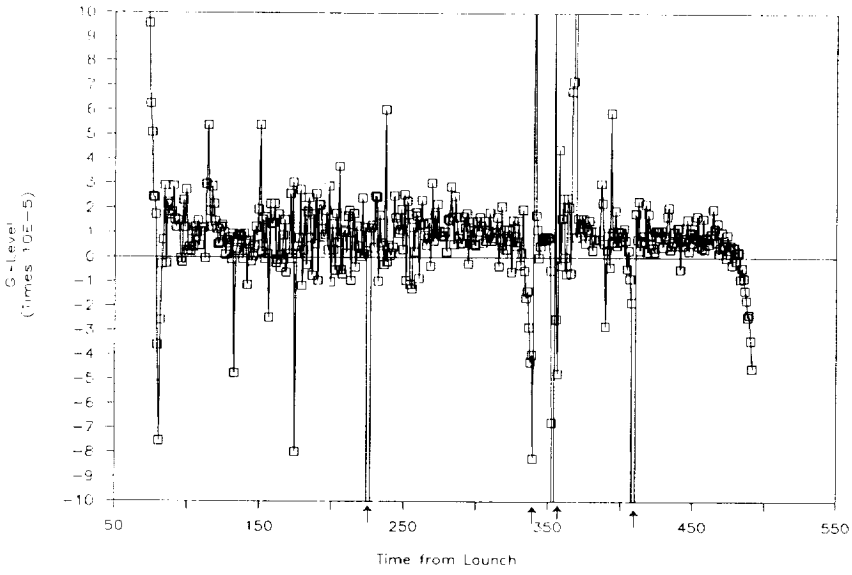

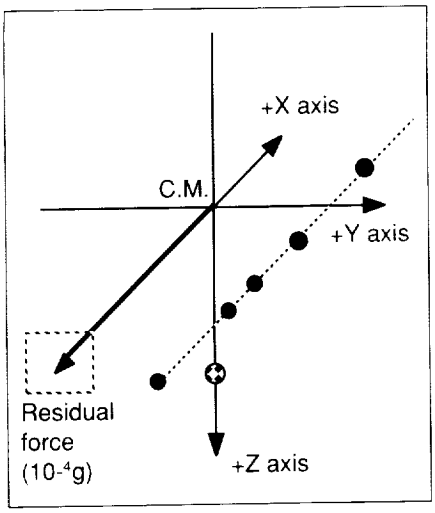


**Figure 4.11-3**
Residual "external" force measured with NASA LGAS accelerometer on Consort 1. To obtain this acceleration, the dotted line indicates the required center of mass for residual roll rates of 0.8 rpm (top right), 1.0, 1.2, 1.4, and fast rpm rates (bottom left).

eration. Since the roll motion was very small and the CM was brought accurately to the center during spin balancing, there is no doubt that the measured accelerations are due to an anomalous force which could be residual off-gassing, an air leak through the non-sealed doors, leaking thrusters, or some other phenomenon.

Finally, detection of the disturbances caused by operating the high-temperature sintering furnace were recorded by the LGAS package. The composite maximum force vector was close to the X-Z plane and was found to be consistent with the design.

### Outlook

It was deduced from the LGAS recording in the X-axis that a sounding rocket flight is very suitable for the accurate calibration of low-g, low-frequency accelerometers, a need which readily became apparent. Neither the Space Shuttle orbiter nor the Space Station can have an entirely drag-free motion, whereas a sounding rocket at apex will achieve an interval of low velocity relative to the air, and also is brought to higher altitudes. The right-hand end of the LGAS X-axis recording shows the drag increase at re-entry. It is evident from this recording, in particular in the X-axis (body axis), that some five minutes of very low gravity conditions ($10^{-6}$ or lower) can be obtained. A further consideration is that sounding rocket onboard activities can be less noisy than those of larger vehicles.

Several complementary activities suggested by these results are:

- Development of disturbance-free experimental hardware such as the use of video cameras, smoothly acting solenoids, etc.
- Development of a standard calibrated microgravity-disturbance measurement fixture for measurements of individual experiments during their development phase, and
- Steps for improving the correlation between measurement and theoretical prediction.

## 4.12 COMMERCIALIZATION OF SPACE FLUIDS MANAGEMENT

**Project:** Program for the commercialization of space fluid management within CMDS

**UAH participants:** Gerald R. Karr, James Kramer, Thomas L. Cost, Ru J. Hung, Mechanical Engineering Department

### Introduction

As the commercialization of space progresses in the next decade, we forsee that a commercial opportunity will exist for the storage and handling of fluids in space. The general concept of this program is the management of fluids in space to make available to all space vehicles (manned or unmanned) the fluids necessary for supporting missions in space and on the lunar surface.

Many different fluids, necessary for various purposes, will be stored and dispersed on demand to vehicles in need of additional propellants, life support fluids or other fluids necessary to support space systems. Future launch systems, for example, could take advantage of the ability to refuel after reaching near-Earth orbit and then to carry payloads to higher orbits or even lunar or planetary destinations. This need for fuel storage and transfer is recognized for many future systems. Examples are storage and transfer of cryogens (liquid nitrogen, oxygen, hydrogen and helium) for use in scientific experimentation, sensor cooling, and life support systems. There also is a need for basic fluid chemicals to be stored in space for chemical processing to produce a wide spectrum of materials required in space manufacture.

This service of providing the various fluids necessary for space operations will result in a cost-effective operation due to the reduced number of supply flights and the more efficient use of space resources.

The NASA Office of Commercial Programs has provided initial funding for exploring these prospects. A 12-month effort was set up that could lead to the establishment of a program for the Commercialization of Space Fluid Management within the CMDS.

The effort is divided into two phases. The first will establish the groundwork for a Workshop on Commercialization of Space Fluid Management in March 1990. The second phase will include the Workshop with subsequent planning and development of the commercialization program. The second phase will also result in establishment of the long-range plans and definition of responsibilities of program members. The major elements of the proposal effort are discussed below.

### Workshop preparation

The major technical issues which must be addressed in the commercialization program are:

- Economic analysis and prediction,
- Fluid management (storage, transfer, handling),
- Space structures and materials,
- Orbital operations and logistics, and
- Safety and reliability.

Phase I began on June 1, 1989, with an intense one-month effort involving review of all existing published material on space fluid management and development of a draft program statement for the proposed commercialization program. This draft program statement is expected to be frequently revised and updated as we proceed through and after the planned workshop. The principal investigator and the co-principal investigators on the program began a detailed economic analysis which required input from other government, university, and industrial elements. An important feature of our analysis is to include the experience of existing commercialization centers. In fact, the final program statement to result from the proposed effort is planned to include close cooperation with other commercialization centers as appropriate. For example, the UAH Center for Space Propulsion, Center for Robotics, and the CMDS are expected to be important partners in this effort.

Planning the workshop was divided among the UAH participants with Karr taking the lead and coordinating with existing consortiums as his major responsibility. Hung led in the recruitment of participants having major interest in the prediction of fluid/vapor/container interactions and transfer mechanics. Cost led in the recruitment of participants having major interest in container manufacture and vehicular control dynamics. Kramer was responsible for development of relationship with selected industrial participants and overall economic analysis. Workshop participants are to be selected to represent the major technical and business issues which face a program for the Commercialization of Space Fluid Management. The major assembly of workshop participants representative of all the relevant technologies that will be focused on Commercialization of Space Fluid Mangement.

### Workshop and program establishment

During the second phase of the planned effort, the workshop will be held March 21-22, 1990. UAH has been very successful in planning and arranging many types of workshops. This workshop will be limited to 50 to 60 participants over a two-day period. The first half-day will consist of a series of presentations on the key technical and business issues facing the Commercialization of Space Fluid Management. In the second half-day, the participants will be divided into smaller working groups which will solicit comments and suggestions on future plans. Participants will move into different subgroups to continue the dialog and development of plans. The team leader in each subgroup will then prepare a summary of the results of the first day's effort. These summa-

ries will be presented to a joint meeting of all workshop participants at the beginning of the second day. The team leaders will meet during the second half of the second day to prepare the final program statement based on the workshop discussions. The goal of the second day is to complete the development of the basic program statement with plans and objectives which have had been reviewed and commented by workshop participants. A written final proceedings of the workshop will be prepared and made available to all participants .

The results of the workshop are expected to give a clear guide to the structure of the commercialization program and its goals. The principal investigator and the co-principal investigators will then begin an effort to develop firm partnership agreements with those groups that best support the goals of the program. These efforts are expected to require considerable involvement of the principal investigator and his co-principal investigators with careful coordination between all parties and potential members. At the end of the second day, plans for the program will be firmly established. It is expected that the program organization can be established and successfully operating with 12 months from the start of this proposed effort.

### Results and conclusion

Since the program was initiated in March more than 14 major briefings have been provided to federal agencies and contractors. Significant interest has been elicited, and conference preparations are on schedule for March.

---

### For additional information

The Consortium for Materials Development in Space is a joint effort of organizations committed to promoting the commercial exploitation of the space environment. The unique attributes of the space environment offer opportunities for materials processing unavailable to Earth-bound endeavors.

Some activities focus on development of specific materials or pilot processes; other address generic processes or equipment for product development; still others pursure space investigations that generate knowledge having economic value to Earth-based materials processes.

The Consortium is partially funded by the National Aeronautics and Space Administration (NASA) Grant #NAGW-812.

For further information, contact:

Director,
Consortium for Materials Development in Space,
R.I., Box 209
The University of Alabama in Huntsville
Huntsville, AL 35899
(☎205-895-6620)

### Acknowledgements

The staff and members of the CMDS wish to thank Felicia Troupe, Linda Jones, and Gail Patterson of UAH for preparing original manuscripts, Dave Dooling of $D^2$ Associates for editing and design, T. Krel Shults for assistance in cover design, UAH Reproduction Services for printing and binding, and the investigators who supplied reports and illustrations.